Geoscience Frontiers 11 (2020) 2323–2337

Contents lists available at ScienceDirect

Geoscience Frontiers

journal homepage: www.elsevier.com/locate/gsf

Research Paper

Record of Early Tonian mafic magmatism in the central Espinhaço (Brazil): New insights for break-up of the Neoproterozoic landmass ancestor of São Francisco-Congo paleocontinent

Helen F. Moreira [a,*], André Danderfer [b], Alice F.O. Costa [b], Samuel M. Bersan [a], Cristiano C. Lana [b], Gláucia N. Queiroga [b]

[a] Post Graduate Program of Department of Geology, Mine School, Federal University of Ouro Preto, Brazil
[b] Department of Geology, Mine School, Federal University of Ouro Preto, Brazil

ARTICLE INFO

Handling Editor: Sohini Ganguly

Keywords:
Mafic rocks
Espinhaço basin
São Francisco-Congo paleocontinent
Tonian rifting
U–Pb geochronology

ABSTRACT

Petrological characterization, U–Pb geochronology, Lu–Hf analyses and major and trace element data from mafic intrusions in the Central Espinhaço (central portion of the Brazilian shield) are used here to investigate the geological significance of the Early Neoproterozoic magmatism in the context of the São Francisco-Congo paleocontinent. These mafic bodies are represented by medium to coarse-grained metagabbros with plagioclase, amphibole and clinopyroxene. Zircon U–Pb isotopic data from two samples yielded weighted mean $^{206}Pb/^{238}U$ ages of 895 ± 3.4 Ma (MSWD = 1.7) and 896 ± 2.4 Ma (MSWD = 0.64), regarded as the best estimates for the crystallization age of these mafic rocks. Major and trace element data (including REEs) show that the gabbros originated from a subalkaline tholeiitic magma, typical of intraplate magmatism. Such rocks are slightly enriched in LREEs and LILEs and depleted in HFSEs. Our new isotope and geochemical data, along with regional knowledge, indicate that these metagabbros mark the beginning of an important Tonian-age extensional tectonic event of the landmass of which the São Francisco-Congo paleocontinent was part (Rodinia supercontinent or Central African block?). We furthermore suggest that these rocks belong to a prominent suite of Tonian-age mafic rocks that mark a diachronic breakup attempt of this landmass which may have occurred from south to north along the Espinhaço mountain range.

1. Introduction

The study of mafic rocks has been applied as powerful tool for paleogeographic reconstructions and geodynamic evolution of crustal fragments or cratons through geologic time (Li et al., 2008; Peng et al., 2011b; Wang et al., 2015; Cederberg et al., 2016; Girardi et al., 2017). According to the "barcode" method proposed by Bleeker and Ernst (2006), originally adjacent crustal fragments are likely to present similar records of their magmatic history and thus produce matching barcodes, whereas the lack of such a match suggests that the fragments were located far from each other during a certain time (e.g., Bleeker and Ernst, 2006; Ernst et al., 2013).

In eastern Brazil, the São Francisco province is the crustal fragment of the so-called São Francisco-Congo paleocontinent, comprising the homonymous craton and the basement of its Neoproterozoic marginal belts (Fig. 1; Almeida, 1977; Alkmim et al., 1993; Danderfer et al., 2015). There is still some debate concerning the positioning of this paleocontinent in the precursor landmass, before the continental fragmentation that took place in the Tonian. In recent paleogeographic reconstructions, the São Francisco-Congo paleocontinent has already been rebuilt either as part of the Rodinia supercontinent (Li et al., 1995, 2008; Fuck et al., 2008; Li and Evans, 2011) or as part of the Central African block (D'Agrela Filho and Cordani, 2017).

The São Francisco province hosts a significant number of intrusive mafic rocks, some of them of Tonian age (e.g., Silva et al., 1995; Carneiro and Oliveira, 2005; Chaves and Neves, 2005; Danderfer et al., 2009; Queiroga et al., 2012; Evans et al., 2016), serving as potential geological markers to better support the issues of reconstruction and positioning of the São Francisco-Congo paleocontinent.

The Espinhaço mountain range is a fold and thrust belt that runs

* Corresponding author. Department of Geology, Mine School, Federal University of Ouro Preto, Brazil, Campus Universitário, 35400-000, Ouro Preto, MG, Brazil.
E-mail addresses: helenfmoreira@yahoo.com.br (H.F. Moreira), danderferandre@gmail.com (A. Danderfer).
Peer-review under responsibility of China University of Geosciences (Beijing).

https://doi.org/10.1016/j.gsf.2020.02.007
Received 9 March 2019; Received in revised form 8 December 2019; Accepted 8 February 2020
Available online 28 February 2020

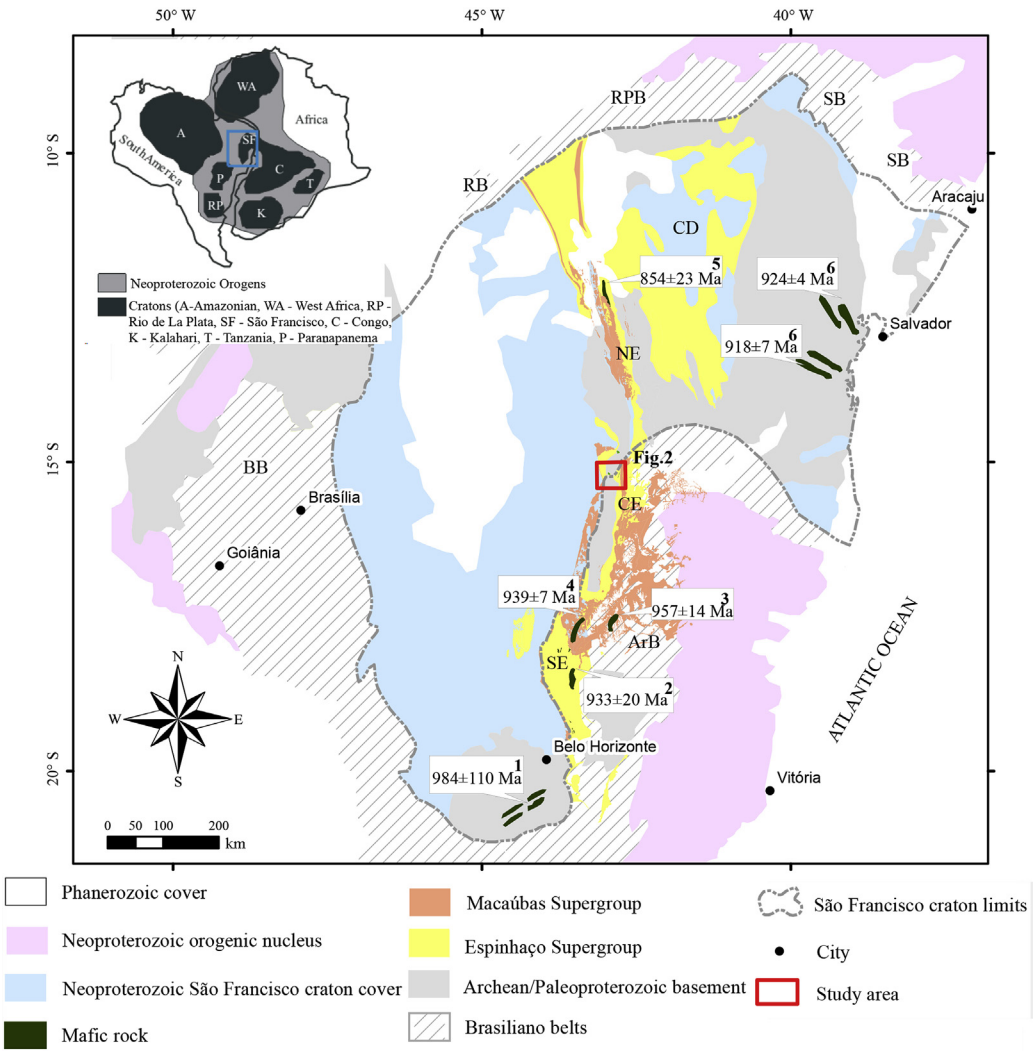

Fig. 1. Geological setting and location of the study area. Some important occurrences of Tonian mafic rocks in the São Francisco craton and Araçuaí belt. (1) Formiga dykes (Sm–Nd – Chaves and Neves, 2005), (2) Southern Espinhaço dykes from Pedro Lessa Suite (U–Pb in zincon – Queiroga et al., 2012), (3) Amphibolites - Capelinha Formation (U–Pb in zircon – Castro et al., 2019), (4) Greenschists (U–Pb in zircon – Souza, 2019), (5) Northern Espinhaço dykes (U–Pb in zincon – Danderfer et al., 2009), (6) Bahia dykes (U–Pb in baddeleyte – Evans et al., 2016). The red square corresponds to the area of Fig. 2 (modified from Danderfer et al., 2015). RPB: Riacho do Pontal Belt; SB: Sergipano Belt; RB: Rio Preto Belt; CD: Chapada Diamantina; NE: Northern Espinhaço; CE: Central Espinhaço; SE: Southern Espinhaço; BB: Brasília Belt; ArB: Araçuaí Belt.

roughly north to south through the eastern portion of the São Francisco province, extending for approximately 1100 km. Numerous intrusive mafic rocks have been mapped and studied throughout the Espinhaço mountain range, especially in its southern and northern portions. However, mafic rocks occurring in the Central Espinhaço lack geochronological and geochemical investigations that may contribute to a better understanding of the tectono-magmatic event responsible for the rupture of the ancestral São Francisco-Congo paleocontinent.

In order to contribute to the definition of a Tonian-age "barcode line" for the Brazilian portion of the São Francisco-Congo supercontinent, we have investigated the U–Pb ages in metagabbros from dykes and a sill in the Central Espinhaço. Also, we carry out an integrated petrographic, geochemical and isotopic (Lu–Hf) study to discuss the petrogenesis, magma sources and tectonic settings of the investigated mafic bodies, as well as their correlations with other records along the eastern São Francisco province. The results presented here contribute to constrain the model of a possible diachronic regional extension of the landmass ancestor of the São Francisco-Congo paleocontinent during the Early Tonian, giving stronger support to the supercontinent reconstructions.

2. Geological setting

The São Francisco province consists of several Archean and Paleoproterozoic terranes, the margins of which were reworked in the Neoproterozoic during Brasiliano/Pan African orogenic event (Almeida, 1977; Romano et al., 2013). It includes a stable cratonic nucleus – the São Francisco craton (SFC) – surrounded by fold-thrust belts (e.g., Araçuaí belt) with basement-involved deformation (Almeida, 1977; Alkmim et al., 1993). The mafic intrusions studied here occur in the Central Espinhaço, which forms part of the external domain of the Araçuaí belt, along the southeastern margin of the São Francisco craton (Fig. 1). It is widely accepted that the São Francisco and the Congo cratons, as well as their marginal belts, constituted a large continental fragment referred to as the São Francisco-Congo paleocontinent (Trompette, 1994; D'Agrella-Filho et al., 1996; Feybesse et al., 1998).

From the tectonic stabilization of its Archean–Paleoproterozoic basement, around 2.0 Ga, until the breakdown and individualization of the São Francisco-Congo paleocontinent, several episodes of intraplate magmatism and related mainly of the rift-type basin formation occurred (e.g., Schobbenhaus, 1993, 1996; Correa-Gomes and Oliveira, 2000; Danderfer and Dardenne, 2002; Danderfer et al., 2009, 2015; Alkmim and Martins-Neto, 2012; Chemale et al., 2012; Guadagnin et al., 2015). In the São Francisco province, many mafic rocks related to this crustal evolution intruded both the Archean–Paleoproterozoic basement and the Meso-Neoproterozoic metasedimentary covers before the breakup in the Tonian (Babinski et al., 1999; Teixeira, 2008; Silveira et al., 2013; Cederberg et al., 2016). Some of these mafic bodies are dykes or form dyke swarms cross-cutting the supracrustal rocks and the basement, others are concordant like sills. Fig. 1 shows some of the main (most relevant for this study) Tonian-age mafic records exposed within the São Francisco Craton and Araçuaí belt.

2.1. Local geology and occurrence of mafic rocks in the study area

The mafic bodies investigated in this paper occur in two different domains. In the eastern portion (Fig. 2), the mafic body is a sill, intrusive in metasedimentary rocks from Sítio Novo Group, with roughly 11 km in length, trending approximately NE–SW and with thickness of ca. 250 m. Samples from this body have been designated here as HMA.

The host rocks of Sítio Novo Group were interpreted as a Stenian-Tonian, rift-fill succession dominated by continental to shallow-marine environment deposition (Schobbenhaus, 1996; Danderfer and Dardenne, 2002; Costa, 2017; Costa and Danderfer, 2017). Detrital zircon U–Pb ages from samples collected in several places along the Sítio Novo Group indicates that its deposition occurred between 950 Ma and 1.1 Ga (Sousa et al., 2014; Costa, 2017; Costa and Danderfer, 2017). Costa and Danderfer (2017) positioned this unit at the base of the Macaúbas Supergroup.

In the western domain (Fig. 2), the mafic rocks appear as discordant bodies (stocks and dykes) crosscutting both the Itacambira-Monte Azul basement rocks and the Sítio Novo Group succession (Knauer et al., 2007; Bersan, 2015). The dykes are up to 150 m thick. Samples of this area have been designated as HGN.

The contacts with the metasedimentary rocks are generally sharp. During the Brasiliano event, these mafic rocks were metamorphosed into low greenschist facies, resulting in metagabbros (Knauer et al., 2007).

3. Analytical methods

The whole-rock chemical compositions of 20 samples from both study domains were analyzed at Acme Analytical Laboratories Ltd. in Vancouver, Canada. To obtain reliable analyses, only the freshest portions of the samples were taken, and any visible evidence of alteration or veining was avoided. Major elements (SiO_2, Al_2O_3, Fe_2O_3, CaO, MgO, Na_2O, K_2O, MnO, TiO_2, P_2O_5, Cr_2O_3 and Ba) were obtained via X-ray fluorescence (XRF). Trace element contents (Ba, Be, Co, Cs, Ga, Hf, Nb, Rb, Sn, Sr, Ta, Th, U, V, W, Zr, Y, La, Ce, Pr, Nd, Sm, Eu, Gd, Tb, Dy, Ho, Er, Tm, Yb, Lu, Mo, Cu, Pb, Zn, Ni, As, Cd, Sb, Bi, Ag, Au, Hg, Tl and Se) were obtained via inductively coupled plasma mass spectrometer (ICP-MS). The detection limits were 0.01 wt.% for oxides and 0.1 ppm for the most trace elements.

Microanalyses of clinopyroxene, plagioclase and amphiboles were performed using a JEOL JXA-8230 electron microprobe at the Microanalysis Laboratory of the Universidade Federal de Ouro Preto. The electron beam was set at 15 kV, 20 nA and 5 μm. Common matrix ZAF corrections were applied. The elements analyzed were Na, Si, Al, Mg, Fe, Ca, F, K, Ti and Mn, using anorthoclase, quartz, gahnite, hypersthene, almandine, fluor-apatite (Ca and F), microcline, rutile and ilmenite as natural standards. Counting times on the peaks/background were 10/5 s for all elements (Na, Si, Al, Mg, Fe, Ca, K), except for F, Ti and Mn (30/15 s). Analytical errors are within 0.21% and 1.43%. All minerals were analyzed with transgranular profiles.

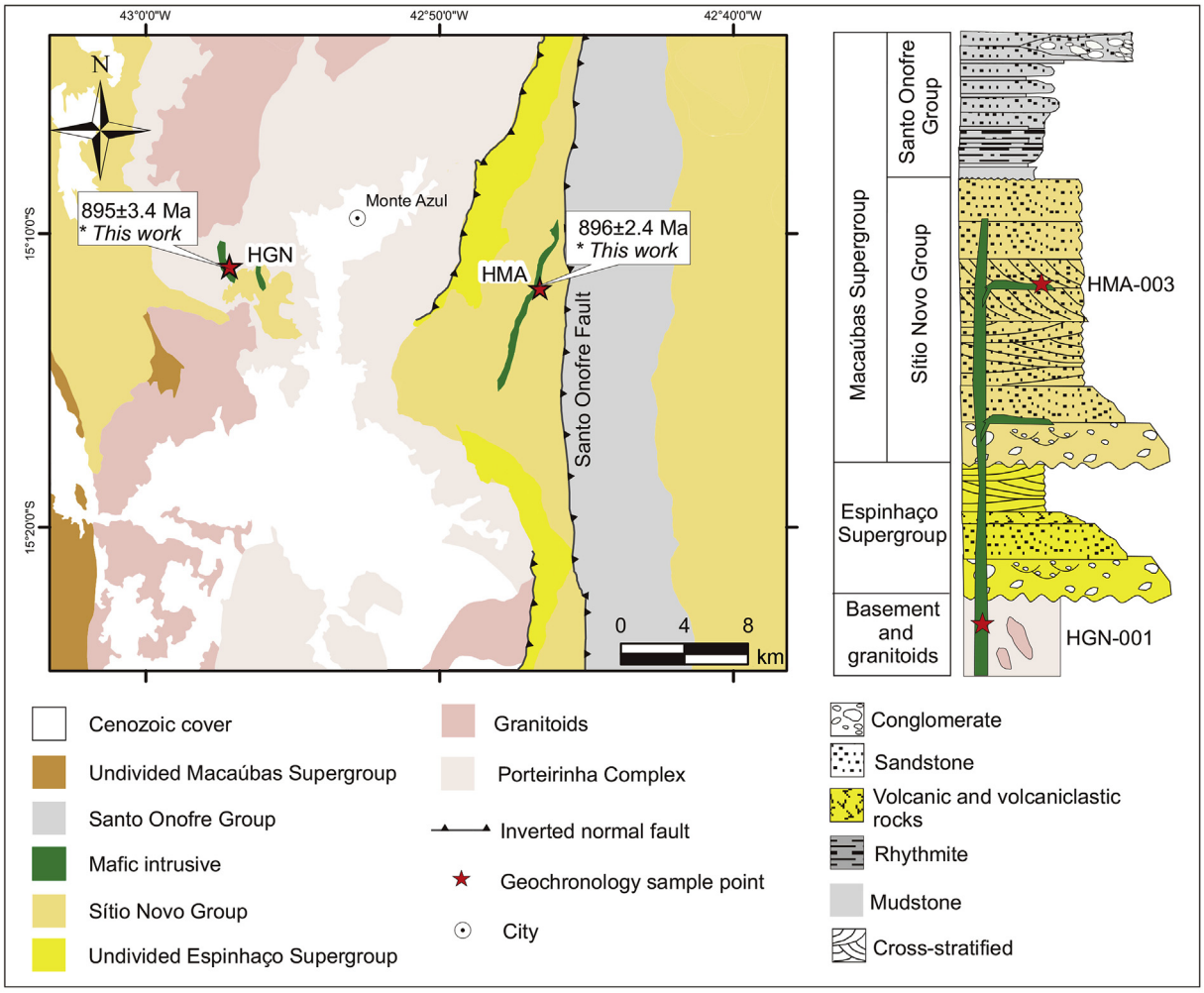

Fig. 2. Local geological map of the area showing the location of mafic bodies and the two domains of study (HMA and HGN). Schematic stratigraphic column is presented in the right (based on Costa, 2017). The star symbols indicate dated samples from the mafic intrusive rocks. Map modified from Costa (2013) and Bersan (2015).

The mineral formulas were calculated based on 6 oxygens atoms in the formula for clinopyroxene, 8 in plagioclase and 23 oxigens in amphibole (total iron as Fe^{2+} according to Leake et al., 1997). The total iron content obtained using the microprobe was normalized as FeO. The binary and ternary diagrams used to characterize the main minerals were plotted using Excel and GCDkit (Janoušek et al., 2006), respectively.

Isotopic analyses of the two zircon-bearing samples were performed using a laser ablation-inductively coupled plasma mass spectrometer (LA-ICPMS) at the Isotope Geochemistry Laboratory of the Universidade Federal de Ouro Preto. Table 1 summarizes some information of the two analyzed samples. The U–Pb ages were obtained in an Element II coupled to a CETAC 213 laser ablation system. The laser spot size was 20 μm. The GLITTER (Van Achterbergh et al., 2001) and Isoplot (Ludwig, 2003) software were used for data processing. Errors for all ages are reported at the 2σ level. GJ (Jackson et al., 2004) and BB (Lana et al., 2017; Santos et al., 2017) were used as primary and secondary standards, respectively (see Supplementary data, Appendixes A.5 and A.7). The Lu–Hf analyses in zircon were obtained using laser ablation multicollector inductively coupled plasma mass spectrometry (LA-MC-ICP-MS, Photon machines 193/Neptune Thermo Scientific) (e.g., Albert et al., 2016; Moreira et al., 2016). GJ (Jackson et al., 2004), BB (Santos et al., 2017) and 91500 (Wiedenbeck et al., 1995) were used as standards, and they were repeatedly measured (see Supplementary data in Appendix A.10) during the analyses of the unknown samples to check the reliability and stability of the instrument. The ^{176}Lu decay constant of 1.867×10^{-11} yr^{-1} provided by Söderlund et al. (2004) was used to calculate the initial $^{176}Hf/^{177}Hf$ ratios.

To calculate $\varepsilon_{Hf}(t)$ values, the chondritic uniform reservoir (CHUR) was used, as recommended by Bouvier et al. (2008); the $^{176}Lu/^{177}Hf$ and $^{176}Hf/^{177}Hf$ ratios were 0.0336 and 0.282785, respectively. The $^{176}Hf/^{177}Hf_{(t)}$ ratios and $\varepsilon_{Hf}(t)$ values of all analyzed zircon spots were calculated using the $^{206}Pb/^{238}U$ ages obtained for the respective domains, except for zircon spots older than 1.0 Ga, for which their respective apparent $^{207}Pb/^{206}Pb$ ages were used.

4. Results

4.1. Petrography and mineral chemistry

The mafic rocks are massive or slightly foliated and without significant internal variations. They are medium grained in the sill (Fig. 3c) and medium to coarse-grained in the HGN domain (Fig. 3b and d). Blocks showing spheroidal weathering are very common (Fig. 3a).

Microscopically, it is possible to recognize metamorphic features, with minerals defining a granonematoblastic texture. The major constituents of these rocks are plagioclase, amphibole and pyroxene. Clinopyroxene (Fig. 4a) are typically altered to amphibole as pseudomorphic grains, and some are completely replaced by small actinolite crystals aggregates (Fig. 4e). Subophitic textures are observed, which are clearly a relict igneous feature (Fig. 4b). A few unaltered crystals (sample HGN-011) were analyzed by EPMA, and the results are presented in the Supplementary data in Appendix A.1. In the Wo-En-Fs ternary diagram (Morimoto, 1988), the pyroxenes are in the augite field (Fig. 5a).

Plagioclase typically displays an igneous tabular habit. It is present as a component of the rock matrix or as larger crystals embedded in the matrix. Some of the tabular crystals have been completely replaced by epidote/clinozoisite due to intense saussuritization. Microprobe analyses (see Supplementary data in Appendix A.2) revealed that the plagioclase grains range compositionally from labradorite ($An_{51.1–64.2}Ab_{31.9–45.9}Or_{0.2–8.6}$) to andesine ($An_{34.7–49.9}Ab_{48.9–64.7}Or_{0.3–3.0}$), as shown in Fig. 5b. Most of the plagioclase crystals are more calcic in their cores than in their rims, i.e., $An_{55–61/Core}$ and $An_{34–64/Edge}$, indicating typical normal crystallization. This pattern is also observed petrographically in the altered grains of plagioclase that experienced the intense substitution of clinozoisite (a calcic mineral) in their cores (Fig. 4c and d).

Table 1
Locations and rock types of samples collected for geochronological analyses.

Sample	Rock type	UTM (E)	UTM (N)
HGN-001	Gabbro	720199	8319624
HMA-003	Gabbro	738428	8318258

Fig. 3. Field occurrence and textures of the mafic bodies from central Espinhaço. (a) Spheroidal weathering; (b–d) variations of texture from medium to coarse-grained.

Amphibole is the main mafic constituent of the studied rocks. It is present as greenish prismatic grains or as aggregates of small acicular crystals that form the groundmass of the rock along with plagioclase. Electron-probe scans indicate that they have a calcic composition (Leake et al., 1997). They were formed from an original magmatic mineral (clinopyroxene). The data from microprobe analyses are presented in the Supplementary data, Appendix A.3. The most Ca-rich amphiboles have the composition of actinolite, but they also reveal compositions of Mg-hornblende and Fe-tschermakite, as is shown in Fig. 6.

Quartz is present as recrystallized grains that together with the amphibole, define a slight foliation in some portions of the rock (Fig. 4f). Chlorite and biotite are present, perhaps as a result of hydrothermal alteration. Magnetite is a common oxide present in almost all thin sections. Other accessory minerals are titanite and zircon.

These rocks consist of mineral assemblages that are typical of low-grade greenschist-facies conditions, although in most samples it is possible to recognize preserved primary textures. All samples were petrographically classified as metagabbro.

4.2. Major and trace element

The major and trace element compositions of samples HGN-001 and HMA-003 are listed in Tables 2 and 3, respectively. The samples from both sites show very similar major oxide compositions. Also the major elements chemistry was not significantly modified by metamorphic processes, as shown by the logarithms oxide molecular proportion ratio (LMPR) diagrams from Beswick and Soucie (1978) (See supplementary data, Appendix A.11). All samples are characterized by low silica and alkali concentrations, with SiO_2 contents ranging from 46.80 wt.% to 48.70 wt.% and $K_2O + Na_2O$ contents ranging from 1.61 wt.% to 2.74 wt.%. The K_2O/Na_2O ratios range from 0.15 to 0.38. Geochemical classification using the $Na_2O + K_2O$ versus SiO_2 (TAS) diagram (Le Bas et al., 1986) shows that the samples plot in the basalt field (Fig. 7) and belong to the subalkaline rock series.

These rocks have tholeiitic affinities (Fig. 8a) and are equivalent to high-Mg tholeiitic basalts (Fig. 8b), with MgO concentrations ranging

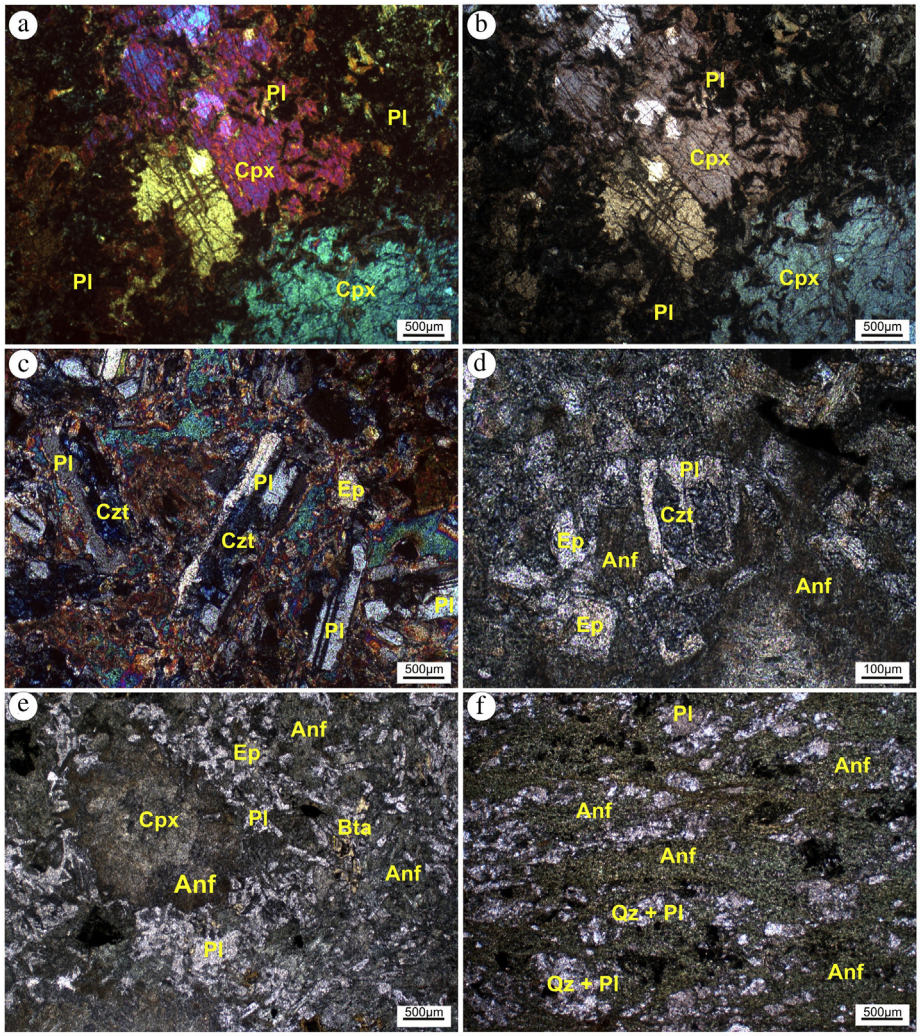

Fig. 4. Photomicrographs of the mafic rocks from the study area. (a) Showing twinned clinopyroxene crystals; (b) subophitic texture with small inclusions of plagioclase in the clinopyroxene; (c) tabular plagioclase showing zonation with clinozoisite in the core; (d) zoned plagioclase exhibiting saussuritization process, with epidote on the edge; (e) pseudmorphic grain of pyroxene partially replaced by amphibole; (f) amphibole, plagioclase and a little quartz slightly foliated. Abbreviations: Cpx–clinopyroxene; Pl–plagioclase; Ep–Epidote; Czt–clinozoisite; Anf–Anfibólio; Bta–Biotite; Qz–quartz.

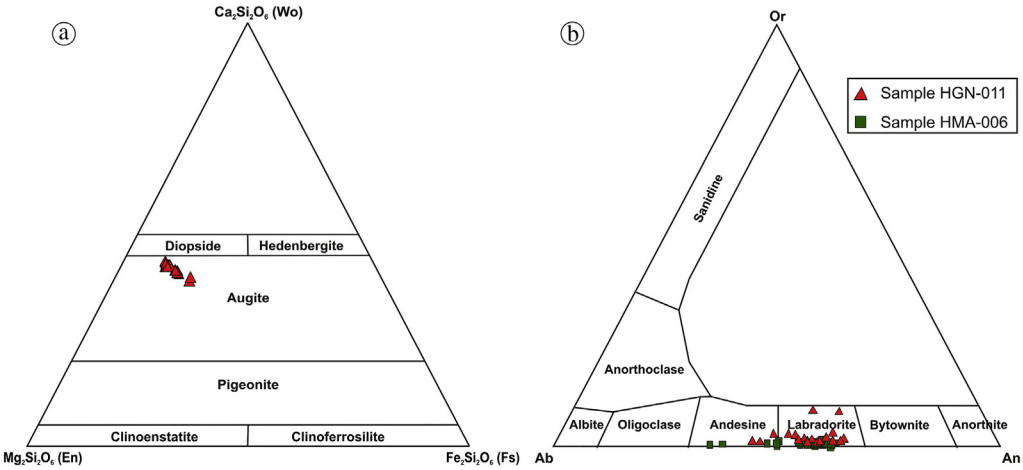

Fig. 5. (a) Plots of clinopyroxenes from sample HGN-011 into the (Entatite–Wollastonite–Ferrossilite) ternary diagram (after Morimoto, 1988). All analyses plot on the augite field. (b) Plots of plagioclase chemistry in the (Albite–Orthoclase–Anorthite) ternary diagram (after Deer et al., 1992).

from 6.95 wt.% to 9.43 wt.%. Their magnesium numbers (Mg#) range from 0.53 to 0.64.

The samples show total rare earth element (REE) contents ranging from 60.32 ppm to 104.24 ppm. On the chondrite-normalized REE diagram of Boynton (1984) (Fig. 9a), the samples show slight fractionation of light rare earth elements (LREEs) relative to heavy rare earth elements (HREEs), with $(La/Yb)_N$ ratios of 3.10 to 4.99. Their Eu/Eu* ratios range from 0.96 to 1.14.

On the primitive-mantle-normalized spider diagram (Fig. 9b), the samples exhibit enrichment in LILEs (large-ion lithophile elements) and

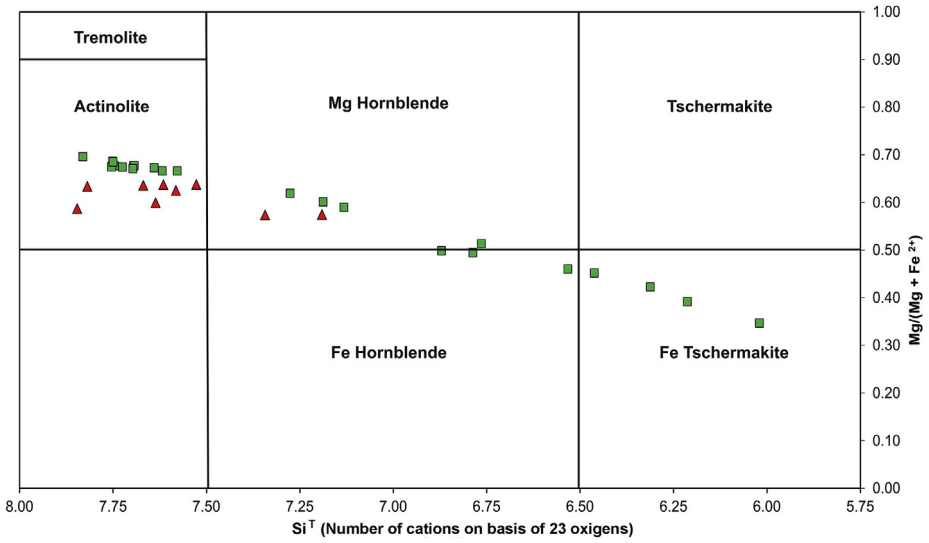

Fig. 6. Plots of Ca-amphiboles from the studied mafic bodies in the IMA classification diagram for Ca-amphiboles (Leake et al., 1997). Red triangles and green squares represent samples from the HGN and HMA domains, respectively.

mobile elements compared to high-field-strength elements (HFSEs).

On the tectonic discriminant diagrams (Fig. 10), the data indicate a within-plate setting. This classification is compatible with the geochemical signature of the rocks typical of intracontinental mafic magmatism. On the binary diagram Zr versus Zr/Y (Fig. 11), the samples are slightly outside of within-plate field, which is probably due to their low Zr content.

4.3. U–Pb dates and Lu–Hf isotopic data

U–Pb isotopic data from samples HGN-001 and HMA-003 are presented in Figs. 12 and 14 and in the Supplementary data (Appendixes A.4 and A.6, respectively). In both samples, it is possible to recognize more than one population of zircons based on their respective ages (Figs. 12 and 14). Two main groups were identified in the sample HGN-001. The first group is characterized by a dark-brown color and the somewhat rounded shapes of the grains. The cathodoluminescence (CL) images of the grains (Fig. 13) reveal well-developed oscillatory zoned cores that yielded the oldest ages (older than 1.8 Ga), and thus are interpreted as xenocrystals. The second group is characterized by abundant euhedral, transparent, colorless grains with prismatic shapes, indicative of a magmatic origin. These grains are elongated crystals with length-to-width ratios ranging from 1:1 to 3:1 and lengths exceeding 70 μm. Forty of these grains gave $^{206}Pb/^{238}U$ dates ranging from 867 Ma to 906 Ma. They cluster near the concordia and yield a $^{206}Pb/^{238}U$ weighted mean age of 895± 3.4 Ma (MSWD = 1.7) (Fig. 12), which is interpreted as the crystallization age of the mafic body represented by sample HGN-001.

In the sample HMA-003, isotopic analyses were obtained from eighty-four spots. Similarly to HGN-001, this sample records a population of zoned cores that gave ages older than 1.8 Ga (Fig. 13). A set of the elongated, transparent, colorless and euhedral grains, some of which showing oscillatory zoning (Fig. 13), gave $^{206}Pb/^{238}U$ ages ranging from 880 Ma to 906 Ma and yield a weighted mean age of 896 ± 2.4 Ma (MSWD = 0.64) (Fig. 14). In other cases, these ages were also obtained from fragments of zircon that may have formed during crystallization. This is a very common feature in mafic rocks due to the relative under-saturation in Zr of the original magma, which produces grains with only partially developed crystal faces (Corfu et al., 2003). Considering the likely magmatic origin of these zircons, a Tonian age is regarded as the best estimate of the crystallization age of the mafic sill represented by sample HMA-003. Among the remaining analyses of sample HMA-003, ten spots yielded younger $^{206}Pb/^{238}U$ ages, i.e., between 504 Ma and 577 Ma, with an average of 543 Ma. These younger ages probably reflect later Pb loss due to post-magmatic processes involving magmatic or inherited grains, as these ages are very discordant with the older respective $^{207}Pb/^{206}Pb$ ages.

For both samples, there are some analyses that are not 100% concordant. Some of the discordant analyses appear to have common Pb contribution, whereas some reversely discordant grains were most likely affected by Pb bias due to matrix effects between sample and reference material. However, these analyses have no significant influence on the results, since the mean age obtained for both samples would be the same, removing these few discordant data.

The Lu and Hf analyses were performed in the same domain of the previous U–Pb spots. The Lu–Hf data present $^{176}Hf/^{177}Hf$ ratios of 0.280790 to 0.282247 for sample HGN-001, and 0.280916 to 0.282299 for sample HMA-003 (Fig. 15a), corresponding to $\varepsilon_{Hf}(t)$ values of −16.6 to +2.28 and −15.5 to +2.9, respectively (Fig. 15b). Despite this variation, most of the grains yield negative ε_{Hf} values, which are compatible with an evolved or moderately juvenile magma (Bahlburg et al., 2011) and may reflect crustal assimilation. No truly juvenile zircons were identified. The vertical arrays of $\varepsilon_{Hf}(t)$ values from zircon grains with ages of ca. 900 Ma suggest that the juvenile magmas of this time interval also assimilated a crustal component.

Most of the older grains (>1.8 Ma), which are probably inherited crystals, show pronounced negative $\varepsilon_{Hf}(t)$ values and lower $^{176}Hf/^{177}Hf$ ratios, indicating long residence times that clearly reflect their crustal composition.

The depleted mantle model age (T_{DM}) obtained from Hf isotope data usually provides a qualitative estimate of the time of segregation of a melt from its source rocks (Bahlburg et al., 2011). However, the probable processes of magmatic differentiation experienced by the magma prior to its crystallization mean that its T_{DM} age may not effectively represent the age of mantle extraction and, therefore, are not considered here.

5. Discussion

5.1. Nature and evolution of the magma source

The geochemical data obtained from the mafic bodies of the Central Espinhaço reveal that these intrusions did not crystallize from a primary basaltic magma. The Mg# (0.53–0.64) and concentrations of transition elements, such as Co (50.6–75.1 ppm), V (237–351 ppm) and Ni (32.4–99.4 ppm) are moderate, however, are lower than those of a

Table 2
Whole-rock chemistry of samples of mafic bodies from HGN domain.

Sample	AS055GQ[a]	AS058GQ[a]	AS060GQ[a]	HGN01-GQ1	HGN01-GQ3	HGN01-GQ4	HGN01-GQ5	HGN02-GQ2	HGN02-GQ3	HGN02-GQ4
Major elements (wt.%)										
SiO_2	47.79	47.56	47.86	47.20	46.80	47.00	47.10	47.70	47.60	47.40
Al_2O_3	15.17	15.23	14.89	15.10	14.20	14.90	15.00	14.60	14.60	14.90
Fe_2O_3	11.47	11.11	11.35	11.00	11.50	11.80	11.20	11.60	11.70	11.00
CaO	11.94	11.94	11.92	12.40	12.00	12.00	12.00	11.60	11.60	12.40
MgO	7.51	7.84	7.62	8.73	9.28	8.19	8.25	7.93	7.87	8.49
Na_2O	1.83	1.76	1.80	1.31	1.21	1.88	1.75	2.02	2.03	1.71
K_2O	0.40	0.47	0.47	0.50	0.40	0.29	0.36	0.56	0.54	0.43
MnO	0.17	0.18	0.17	0.18	0.18	0.18	0.18	0.18	0.18	0.17
TiO_2	1.58	1.48	1.56	1.46	1.41	1.57	1.51	1.62	1.62	1.51
P_2O_5	0.18	0.17	0.18	0.17	0.16	0.19	0.18	0.20	0.19	0.17
Cr_2O_3	-	-	-	0.04	0.03	0.03	0.04	0.04	0.04	0.04
Ba	-	-	-	0.01	< 0.01	0.04	0.02	0.01	0.01	0.01
LOI	2.10	2.38	2.12	2.33	2.44	2.32	2.39	1.90	1.89	2.10
SUM	100.15	100.11	99.94	100.43	99.61	100.39	99.98	99.96	99.87	100.33
Trace elements (ppm)										
Ba	152.00	132.00	112.00	135.00	111.00	409.00	185.00	164.00	167.00	156.00
Be	0.00	0.00	1.00	< 1.00	< 1.00	< 1.00	< 1.00	1.00	2.00	2.00
Co	61.40	56.90	57.90	60.50	54.80	56.00	50.60	52.50	51.50	61.10
Cs	0.50	0.80	0.90	0.20	0.20	0.20	0.20	0.20	0.20	0.30
Ga	17.20	16.40	16.50	15.30	14.20	14.30	14.30	14.40	14.70	14.30
Hf	2.50	2.10	2.80	2.30	2.00	2.10	2.40	2.30	2.70	2.20
Nb	10.10	9.10	10.10	7.50	8.00	8.90	8.60	9.50	9.80	8.40
Rb	9.30	9.50	11.80	10.10	7.80	6.50	8.30	11.90	10.70	8.00
Sn	< 1.00	< 1.00	< 1.00	< 1.00	< 1.00	< 1.00	< 1.00	2.00	< 1.00	< 1.00
Sr	288.50	257.70	252.00	257.90	231.60	279.30	295.50	254.40	241.40	290.80
Ta	0.60	0.70	0.60	0.50	0.50	0.60	0.60	0.70	0.60	0.50
Th	0.80	0.70	0.90	0.60	0.60	0.80	0.90	0.80	1.00	0.80
U	0.20	0.20	0.20	0.20	0.20	0.10	0.20	0.20	0.20	0.20
V	290.00	267.00	288.00	252.00	244.00	263.00	268.00	273.00	280.00	274.00
W	128.10	101.60	111.00	120.70	29.20	45.10	42.00	44.20	48.70	55.30
Zr	105.60	88.10	97.80	76.90	82.40	92.50	92.20	100.30	103.60	88.40
Y	19.30	18.60	20.00	19.10	19.80	22.70	22.40	20.60	21.20	19.50
La	12.80	10.40	12.10	10.20	10.10	13.80	12.30	12.60	12.10	10.50
Ce	26.00	23.00	26.60	22.50	22.00	28.00	26.70	28.50	28.60	23.30
Pr	3.50	3.06	3.27	3.09	2.89	4.32	3.70	3.63	3.68	3.28
Nd	14.90	13.10	15.80	14.10	13.60	17.60	15.70	16.20	16.20	14.70
Sm	3.55	3.23	3.57	3.37	3.43	4.61	3.72	3.90	3.68	3.39
Eu	1.22	1.17	1.24	1.25	1.17	1.58	1.47	1.32	1.44	1.31
Gd	4.01	3.79	3.97	3.76	3.81	4.99	4.17	4.16	4.21	3.75
Tb	0.62	0.55	0.59	0.63	0.65	0.86	0.74	0.73	0.74	0.68
Dy	4.07	3.54	3.59	3.64	3.49	4.88	4.14	4.18	4.24	3.67
Ho	0.76	0.72	0.83	0.90	0.78	1.02	0.89	0.99	0.92	0.80
Er	2.25	1.83	1.87	2.45	2.39	3.07	2.55	2.85	2.55	2.27
Tm	0.32	0.29	0.29	0.33	0.30	0.40	0.37	0.36	0.35	0.35
Yb	1.73	1.88	1.92	2.12	2.10	2.66	2.29	2.25	2.37	1.93
Lu	0.33	0.26	0.27	0.29	0.27	0.38	0.33	0.35	0.36	0.30
Mo	-	-	-	0.40	0.30	0.30	0.30	0.50	0.50	0.30
Cu	-	-	-	128.10	161.90	108.00	80.40	111.60	116.90	111.40
Pb	-	-	-	0.80	0.70	0.60	0.40	0.60	0.60	0.80
Zn	-	-	-	40.00	41.00	42.00	40.00	40.00	39.00	36.00
Ni	-	-	-	89.60	99.40	77.10	68.20	61.90	63.10	70.90
As	-	-	-	< 0.50	< 0.50	0.70	< 0.50	< 0.50	0.60	< 0.50
Cd	-	-	-	< 0.10	< 0.10	< 0.10	< 0.10	< 0.10	< 0.10	< 0.10
Sb	-	-	-	< 0.10	< 0.10	< 0.10	< 0.10	< 0.10	< 0.10	< 0.10
Bi	-	-	-	< 0.10	< 0.10	< 0.10	< 0.10	< 0.10	< 0.10	< 0.10
Ag	-	-	-	< 0.10	< 0.10	< 0.10	< 0.10	< 0.10	< 0.10	< 0.10
Au	-	-	-	1.50	11.50	0.90	0.70	1.00	1.30	1.00
Hg	-	-	-	< 0.01	< 0.01	< 0.01	< 0.01	< 0.01	< 0.01	< 0.01
T1	-	-	-	< 0.10	< 0.10	< 0.10	< 0.10	< 0.10	< 0.10	< 0.10
Se	-	-	-	< 0.50	< 0.50	< 0.50	< 0.50	< 0.50	< 0.50	< 0.50
Parameters										
$Na_2O + K_2O$	2.23	2.23	2.27	1.81	1.61	2.17	2.11	2.58	2.57	2.14
K_2O/Na_2O	0.22	0.27	0.26	0.38	0.33	0.15	0.21	0.28	0.27	0.25
FeO[b]	10.32	10.00	10.21	9.90	10.35	10.62	10.08	10.44	10.53	9.90
Mg#	0.56	0.58	0.57	0.61	0.62	0.58	0.59	0.58	0.57	0.60
∑REE	76.06	66.82	75.91	68.63	66.98	88.17	79.07	82.02	81.44	70.23
$(La/Yb)_N$	4.99	3.73	4.25	3.24	3.24	3.50	3.62	3.78	3.44	3.67
Eu/Eu*[c]	0.99	1.02	1.00	1.07	0.99	1.00	1.14	1.00	1.12	1.12

[a] Samples provided by Bersan (2015).
[b] $FeO = Fe_2O_3 \times 0.8998$.
[c] $Eu/Eu^* = 2Eu_N/(Sm_N + Gd_N)$, N denotes normalized to chondrite from Boynton (1984).

Table 3
Whole-rock chemistry of samples of mafic bodies from HMA domain. Major (%) and trace element (ppm) concentrations.

Sample	OPU 4013[a]	HMA03-GQ1	HMA03-GQ2	HMA03-GQ3	HMA04-GQ1	HMA04-GQ2	HMA04-GQ3	HMA05-GQ1	HMA05-GQ2	HMA05-GQ4
Major elements (wt.%)										
SiO_2	48.02	48.30	48.50	48.50	48.30	48.70	47.50	47.70	47.70	48.00
Al_2O_3	14.81	15.00	15.60	15.00	15.20	14.40	15.30	15.70	15.90	15.90
Fe_2O_3	11.97	11.30	11.10	11.60	10.80	12.40	10.30	10.60	10.80	10.90
CaO	11.66	12.40	12.20	12.30	12.50	12.20	12.60	12.50	12.30	12.40
MgO	7.99	7.97	7.45	7.93	8.55	6.95	9.43	8.82	9.00	8.84
Na_2O	2.08	2.16	2.32	2.24	2.04	2.29	1.75	2.09	1.97	2.03
K_2O	0.43	0.38	0.42	0.39	0.31	0.39	0.29	0.32	0.31	0.33
MnO	0.18	0.19	0.19	0.19	0.18	0.24	0.16	0.18	0.17	0.18
TiO_2	1.63	1.43	1.51	1.39	1.48	1.97	1.25	1.35	1.31	1.37
P_2O_5	0.18	0.16	0.19	0.16	0.17	0.25	0.14	0.16	0.15	0.16
Cr_2O_3	0.03	0.03	0.02	0.03	0.07	0.02	0.07	0.04	0.04	0.05
Ba	0.01	< 0.01	0.02	0.01	0.01	0.02	< 0.01	0.01	0.01	0.02
LOI	1.55	0.70	0.62	0.81	1.01	0.65	1.79	0.83	0.53	0.43
SUM	100.54	100.02	100.14	100.55	100.62	100.48	100.58	100.30	100.19	100.61
Trace elements (ppm)										
Ba	116.00	136.00	157.00	159.00	119.00	158.00	89.00	125.00	128.00	140.00
Be	2.00	< 1.00	< 1.00	< 1.00	2.00	2.00	< 1.00	1.00	1.00	3.00
Co	75.10	54.30	56.90	56.00	58.50	51.10	51.60	64.60	57.80	69.10
Cs	0.50	0.30	0.40	0.40	0.20	0.30	0.50	< 0.10	0.30	0.20
Ga	16.30	13.40	14.40	13.60	13.80	15.70	13.30	14.20	13.90	14.10
Hf	2.90	2.10	2.50	2.00	2.30	3.40	2.00	1.90	2.00	2.00
Nb	10.80	7.80	9.00	7.20	8.40	11.80	7.30	7.50	7.20	7.90
Rb	7.60	6.00	7.60	5.80	4.20	5.90	5.70	5.00	5.20	5.40
Sn	< 1.00	< 1.00	< 1.00	< 1.00	< 1.00	< 1.00	< 1.00	< 1.00	< 1.00	< 1.00
Sr	258.70	271.80	259.40	256.30	231.30	243.90	305.40	252.00	239.00	246.90
Ta	0.80	0.60	0.60	0.60	0.60	0.80	0.50	0.50	0.50	0.70
Th	1.00	0.70	0.70	1.00	0.80	1.30	0.70	0.60	0.70	0.70
U	0.40	0.20	0.10	0.20	0.20	0.20	0.20	0.20	0.10	0.20
V	311.00	245.00	261.00	269.00	271.00	351.00	237.00	242.00	242.00	251.00
W	204.50	99.60	106.30	110.70	90.90	90.30	64.20	171.20	92.90	113.50
Zr	115.20	86.20	97.10	82.10	95.30	132.90	75.40	80.50	75.70	85.20
Y	20.60	19.30	19.40	19.00	18.90	26.80	14.80	16.20	15.80	16.80
La	13.30	9.70	12.70	10.30	11.40	15.70	9.60	9.50	9.50	9.30
Ce	28.10	23.60	24.50	22.40	23.00	35.80	21.00	23.00	20.30	22.60
Pr	3.57	3.10	3.43	3.06	3.12	4.87	2.69	2.93	2.81	2.97
Nd	15.80	13.20	14.80	13.20	15.30	21.20	11.50	14.10	12.20	13.90
Sm	3.89	3.39	3.43	3.28	3.43	4.74	2.74	3.26	3.08	3.00
Eu	1.30	1.29	1.31	1.26	1.19	1.60	0.95	1.13	1.19	1.12
Gd	4.19	3.70	4.00	3.78	3.89	5.53	3.19	3.45	3.35	3.38
Tb	0.67	0.64	0.68	0.69	0.65	0.96	0.56	0.60	0.56	0.58
Dy	4.17	3.48	3.96	3.60	3.89	5.33	3.10	3.26	3.27	3.26
Ho	0.75	0.79	0.80	0.82	0.86	1.18	0.67	0.71	0.67	0.71
Er	2.17	2.32	2.43	2.40	2.34	3.36	2.01	2.18	1.93	2.00
Tm	0.30	0.31	0.35	0.32	0.33	0.46	0.28	0.30	0.28	0.28
Yb	2.03	2.11	2.14	2.04	2.11	3.07	1.75	2.04	1.85	1.79
Lu	0.30	0.30	0.32	0.28	0.31	0.44	0.28	0.29	0.23	0.28
Mo	0.40	0.30	0.30	0.30	0.30	0.40	0.20	0.30	0.30	0.30
Cu	105.20	115.70	107.70	133.90	107.80	140.00	79.10	77.30	97.20	94.60
Pb	0.80	1.60	1.20	2.90	3.00	3.20	1.10	20.20	3.90	4.60
Zn	28.00	27.00	26.00	34.00	23.00	43.00	21.00	20.00	23.00	23.00
Ni	54.20	38.90	36.90	40.50	47.80	32.40	71.60	56.10	65.40	58.90
As	< 0.50	0.60	< 0.50	< 0.50	0.50	< 0.50	< 0.50	1.20	< 0.50	0.50
Cd	< 0.10	< 0.10	< 0.10	< 0.10	< 0.10	0.10	< 0.10	0.20	< 0.10	< 0.10
Sb	< 0.10	< 0.10	< 0.10	< 0.10	< 0.10	< 0.10	< 0.10	< 0.10	< 0.10	< 0.10
Bi	< 0.10	< 0.10	< 0.10	< 0.10	< 0.10	< 0.10	< 0.10	< 0.10	< 0.10	< 0.10
Ag	< 0.10	< 0.10	< 0.10	< 0.10	< 0.10	< 0.10	< 0.10	< 0.10	< 0.10	< 0.10
Au	1.40	0.70	0.60	1.00	< 0.50	0.90	0.50	0.70	0.50	< 0.50
Hg	< 0.01	< 0.01	< 0.01	< 0.01	< 0.01	< 0.01	< 0.01	< 0.01	< 0.01	< 0.01
Tl	< 0.10	< 0.10	< 0.10	< 0.10	< 0.10	< 0.10	< 0.10	< 0.10	< 0.10	< 0.10
Se	< 0.50	< 0.50	< 0.50	< 0.50	< 0.50	< 0.50	< 0.50	< 0.50	< 0.50	< 0.50
Parameters										
$Na_2O + K_2O$	2.51	2.54	2.74	2.63	2.35	2.68	2.04	2.41	2.28	2.36
K_2O/Na_2O	0.21	0.18	0.18	0.17	0.15	0.17	0.17	0.15	0.16	0.16
FeO[b]	10.77	10.17	9.99	10.44	9.72	11.16	9.27	9.54	9.72	9.81
Mg#	0.57	0.58	0.57	0.58	0.61	0.53	0.64	0.62	0.62	0.62
∑REE	80.54	67.93	74.85	67.43	71.82	104.24	60.32	66.75	61.22	65.17
$(La/Yb)_N$	4.42	3.10	4.00	3.40	3.64	3.45	3.70	3.14	3.46	3.50
Eu/Eu*[c]	0.98	1.11	1.08	1.09	0.99	0.95	0.98	1.02	1.13	1.07

[a] Samples provided by Costa (2013).
[b] $FeO = Fe_2O_3 \times 0.8998$.
[c] $Eu/Eu^* = 2Eu_N/(Sm_N + Gd_N)$, N denotes normalized to chondrite from Boynton (1984).

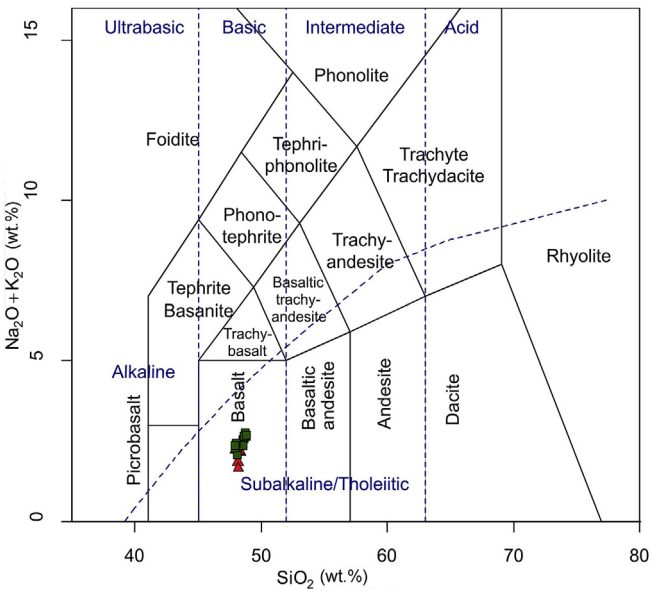

Fig. 7. TAS diagram from Le Bas et al. (1986). Red triangles and green squares represent samples from the HGN and HMA domains, respectively.

primary melt (Wilson, 1989), indicating that the original magma underwent some process of fractional crystallization, probably inside magma chambers, prior to its emplacement (Zhu et al., 2011).

In addition to fractional crystallization, differentiation may also be associated with some assimilation of crustal material, as indicated by the negative ε_{Hf} values, the positive Ba anomalies and slight enrichment in lithophile elements (LILEs), such as K and Rb.

As mentioned earlier, samples from the HMA and HGN domains are geochemically very similar (Fig. 9). Fig. 16 shows that the two sets of samples are very similar in terms of the correlations between their Ti and Zr concentrations (both are incompatible elements), suggesting that the mafic bodies in the two domains may have crystallized from the same source of magma. The Lu–Hf isotopic compositions also support this conclusion. In general, the geochemical characteristics reflect sources that are more enriched than N-MORB basalts and similar to enriched mid-ocean ridge basalts (E-MORB).

5.2. Regional correlation

The new crystallization ages of ca. 895 Ma and 896 Ma obtained from the Central Espinhaço mafic rocks are similar to the data obtained from other mafic intrusions that occur along the Espinhaço mountain range. Tonian-age mafic rocks in the southern Espinhaço were first reported by Machado et al. (1989) who dated baddeleyite grains from mafic sills located near Pedro Lessa city (in the State of Minas Gerais) and obtained

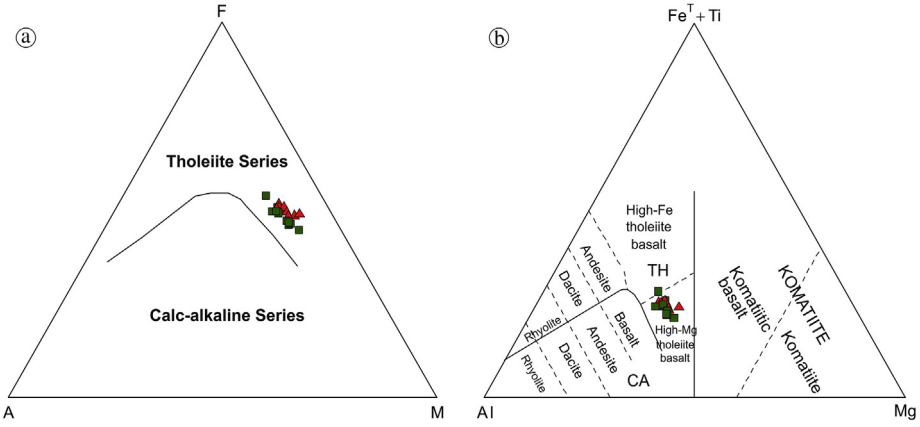

Fig. 8. Geochemical diagram. (a) AFM ternary diagram after Irvine and Baragar (1971); (b) Fe^T + Ti–Al–Mg ternary diagram after Jensen (1976). Red triangles and green squares represent samples from the HGN and HMA domains, respectively.

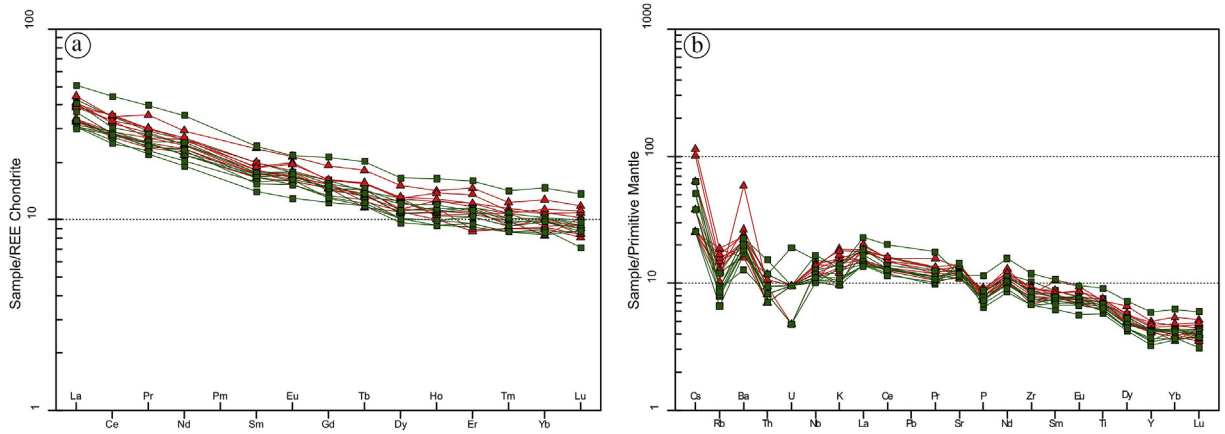

Fig. 9. (a) Chondrite-normalized REE patterns (Boynton, 1984); (b) primitive mantle-normalized trace element patterns (Sun and Mcdonough, 1989). Red triangles and green squares represent samples from the HGN and HMA domains, respectively. Curves of OIB (oceanic island basalts); N-MORB (normal mid ocean ridge basalts) and E-MORB (enriched mid ocean ridge basalts) are shown as reference (Sun and Mcdonough, 1989).

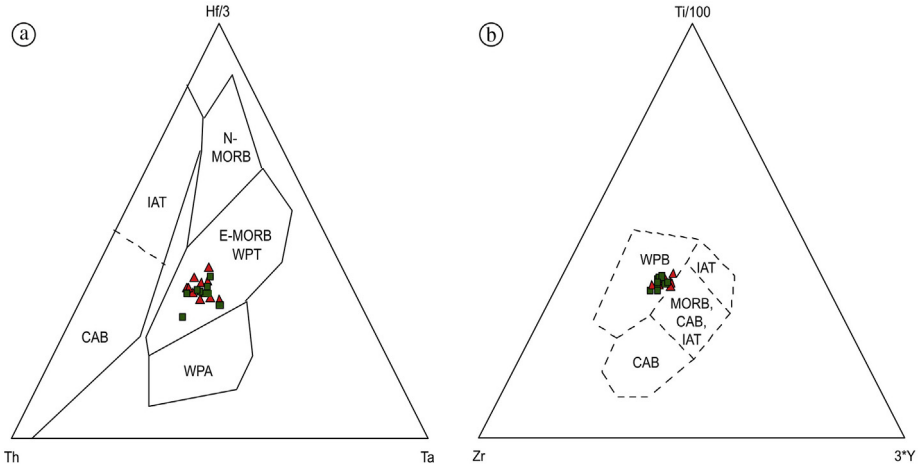

Fig. 10. Geotectonic diagrams. (a) Ternary Th–Hf/3–Ta diagram (after Wood, 1980); (b) ternary Zr–Ti/100–3*Y diagram (after Pearce and Cann, 1973). Symbols are the same as those in Fig. 8.

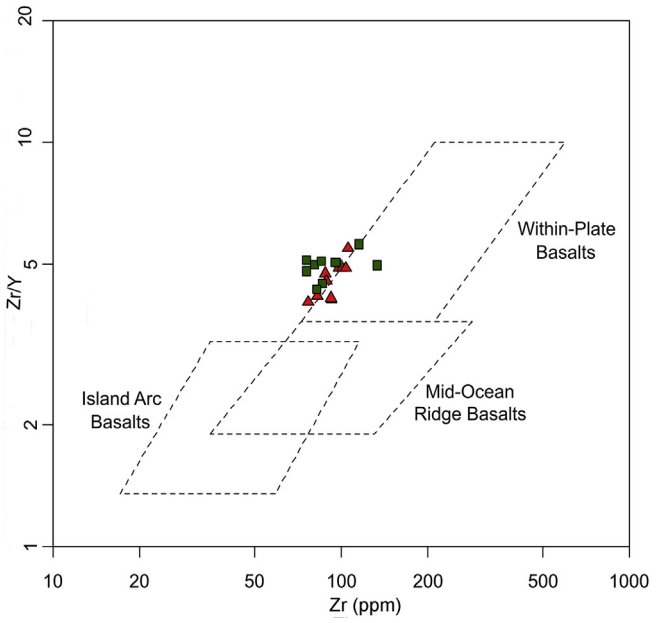

Fig. 11. Geotectonic diagram Zr vs. Zr/Y (Pearce and Norry, 1979).

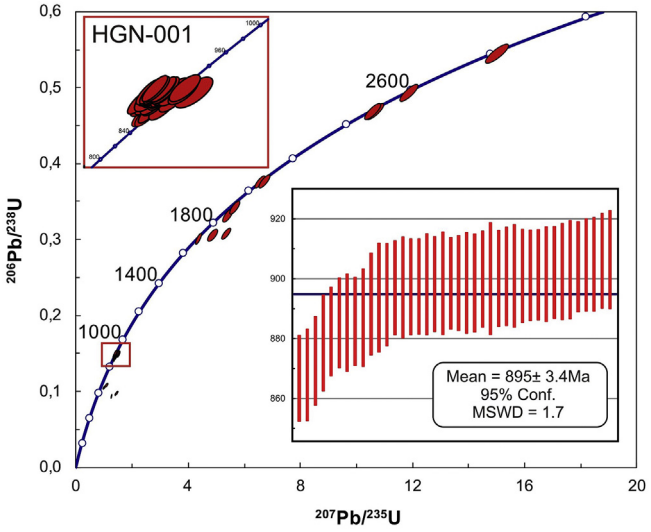

Fig. 12. Zircon LA-ICP-MS U–Pb concordia diagram showing the different populations of ages from sample HGN-001 and the weighted mean $^{206}Pb/^{238}U$ ages, taken as the best estimate of the crystallization age.

a crystallization age of 906 ± 2.0 Ma. Since then, many other mafic bodies have been mapped in this region and assigned to the so-called, Pedro Lessa Suite, which encompasses these Tonian-age mafic intrusions. Later, Queiroga et al. (2012) redefined the crystallization age of the mafic rocks of Pedro Lessa Suite at 933 ± 20 Ma, based on more robust U–Pb data from zircon grains (Fig. 1).

In the northern Espinhaço, mafic intrusions have also been reported. However, the only Tonian-age was presented by Danderfer et al. (2009) who dated zircon grains from mafic dykes using U–Pb SHIRIMP method, which yielded a crystallization age of 854 ± 23 Ma (Fig. 1).

Tonian ages have also been assigned for deformed mafic rocks in other domains of the Araçuaí belt, southeast of São Francisco craton (SFC) (Uhlein, 1991; Chula, 1996; Gradim et al., 2005; Souza, 2016; Castro et al., 2019). Souza (2019) presented a crystallization age of 939 ± 7 Ma from a greenschist sample which was interpreted as record of the same mafic magmatism that originated the metagabbros of the Pedro Lessa Suite.

In the southern SFC, Tonian-age mafic dykes comprise the Formiga swarm in the State of Minas Gerais (Fig. 1). These dykes revealed isochron ages of 984 ± 110 Ma (Sm–Nd) (Chaves and Neves, 2005) and 940 ± 50 Ma (Ar–Ar) (Carneiro and Oliveira, 2005). Chaves et al. (2014) had already demonstrated the petrographic and geochemical similarities between the Formiga mafic dykes and those comprising Pedro Lessa Suite in the southern Espinhaço.

The multi-element diagrams in Fig. 17 compare the data obtained from mafic bodies of this study and data from the Formiga and Pedro Lessa metagabbros (Queiroga et al., 2012; Chaves et al., 2014). The samples reveal very similar patterns of REEs and other incompatible elements, thus, supporting the conclusion that the mafic bodies in the central Espinhaço can be associated with the same Tonian magmatism that produced the Pedro Lessa and Formiga mafic dykes (Fig. 1).

5.3. Tectonic implications

Despite some small variations in the geochemical characteristics of the Tonian-age mafic rocks in the southern São Francisco craton and Araçuaí belt, obtained from metagabbros, greenschists and amphibolites (Tanner de Oliveira, 1989; Uhlein, 1991; Chula, 1996; Gradim et al., 2005; Danderfer et al., 2009; Chaves et al., 2014; Castro et al., 2019; Souza, 2019), all these mafic bodies point to an origin from subalkaline

Fig. 13. Cathodoluminescence (CL) images from zircon grains showing their morphological aspects.

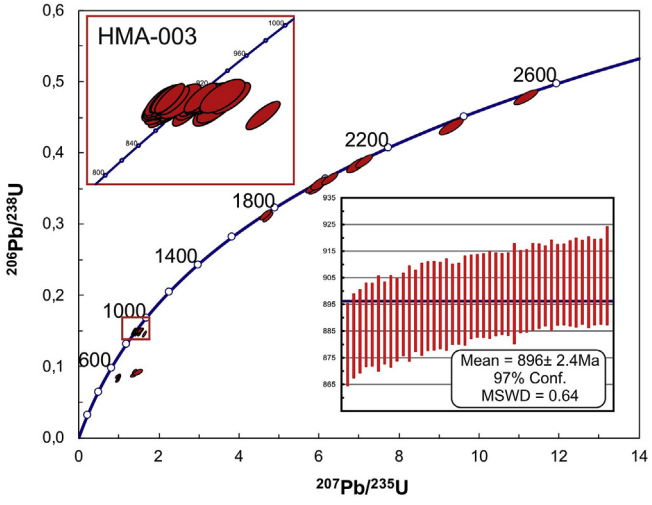

Fig. 14. Zircon LA-ICP-MS U–Pb concordia diagram showing the different populations of ages from sample HMA-003 and the weighted mean $^{206}Pb/^{238}U$ ages, taken as the best estimate of the crystallization age.

basaltic magmas, with tholeiitic affinity, typical of intraplate magmatism. Thus, they can all be interpreted as records of a large-scale mafic magmatism caused by significant crustal extension that affected the eastern border São Francisco block (SFC and Araçuaí marginal belt) during the Tonian.

In a regional framework, these mafic rocks can be related to the extensional event that paved the way to deposition of a large Neoproterozoic intracratonic basin, known as the Macaubas Basin (Pedrosa-Soares et al., 2011; Babinski et al., 2012). The Macaubas basin evolution involved two rifting stages before the passive margin partially floored by oceanic crust (Kuchenbecker et al., 2015; Alkmim et al., 2017). In the bottom of the Macaúbas sequence, Castro et al. (2019) dated amphibolites of the Capelinha Formation and obtained a crystallization age of 957 ± 14 Ma, which was interpreted as the first record of the Tonian magmatism, syndepositional to the development of the initial rifting in this basin.

Along the Espinhaço mountain range, the Tonian-age mafic rocks become progressively younger northward, ranging from mafic rocks in the southern Espinhaço (~933 Ma), going towards slightly younger (~900 Ma) mafic intrusions in the central Espinhaço to the youngest age (~850 Ma, Danderfer et al., 2009) in the northern end (Fig. 1).

Therefore, this scenario can be interpreted as a result of a diachronic rifting that might have been developed from south to north, affecting the Espinhaço basin in different stages during the Tonian, marking breakup attempts. This rifting that occurred differently both in time and space would be analogous to the diachronic fragmentation that occurred during the Phanerozoic and led to the opening of the Atlantic Ocean and rupture of the Gondwana Continent (Carneiro et al., 2012).

Similar records of Tonian-age magmatism also have been reported for

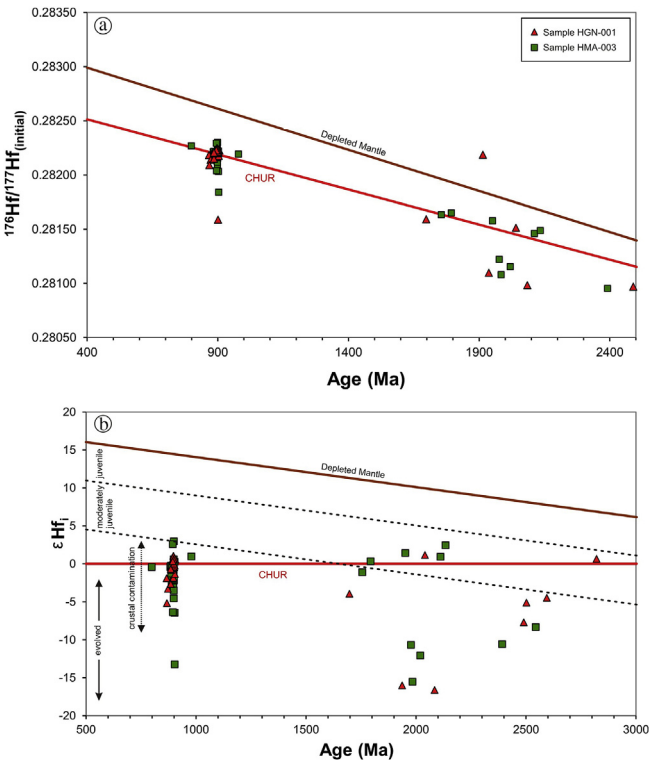

Fig. 15. (a) Zircon Lu–Hf isotopic compositions from samples HGN-001 and HMA-003; (b) ε_{Hf} obtained from the Hf compositions of samples HGN-001 and HMA-003. The fields: juvenile, moderately juvenile and evolved are from Bahlburg et al. (2011).

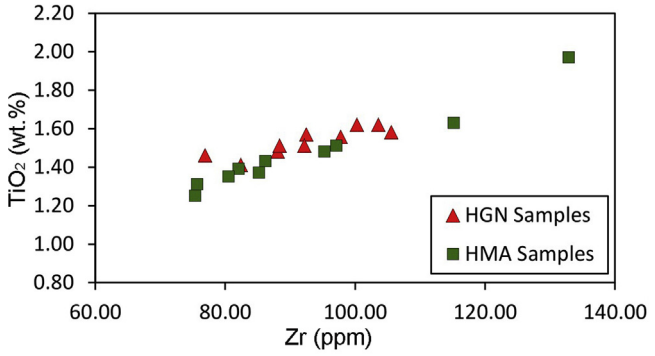

Fig. 16. Zr vs. TiO_2 diagram for HGN and HMA samples (based on Teixeira, 2008).

other continental pieces, such as the Congo and North China cratons. In the West Congo craton, there are significant volcanic mafic rocks of ca. 920 Ma, such as the Gangila basalts, typical continental flood basalts (Tack et al., 2001). Chaves et al. (2014) correlated the mafic dykes from Formiga and Pedro Lessa Suite with those of Kinga-Comba and Sembé Ouesso (Vicat and Pouclet, 1995), which are also located in the Congo craton.

In the North China craton (NCC), ages of approximately 925 Ma (baddeleyite U–Pb) have been reported by Peng et al. (2011b) for the mafic dykes comprising the Dashigou swarm. Also, the ca. 900 Ma Chulan-Dalian sills occur along the southern margin of the eastern NCC, associated with rocks of the Xu–Huai Rift System (Peng et al., 2011a).

Peng et al. (2011b) suggested that together, these ~925 Ma dykes and ~900 Ma sills constitute a large igneous province (LIP) that was produced by a Neoproterozoic mantle plume. In addition, they have proposed a connection model between the North China craton and the São Francisco-Congo paleocontinent, where this same mantle plume would be associated with the emplacement of the Bahia dykes (Evans et al., 2016) (Fig. 1) and Gangila volcanic rocks, in the São Francisco and Congo cratons, respectively.

Recently, Chaves et al. (2018) characterized the geochemical data of the so-called Bahia-Gangila LIP (that includes rocks of the Pedro Lessa suite, Formiga swarm and others that they considered to be associated to this LIP) and compared with those of the Dashigou-Chulan LIP from the North China craton (Peng et al., 2011b). The samples reveal a subalkaline and tholeiitic composition (Fig. 18), indicative of within-plate setting. The multi-element diagrams shown in Fig. 19 exhibit some relevant differences related to incompatible elements concentrations. Even so, the results presented by Chaves et al. (2018) demonstrate similarities between the magmas that originated these occurrences.

The correlation between the geochemical data provides additional support for the hypothesis of connection of São Francisco, Congo and North China cratons, although the model originally proposed by Peng et al. (2011b) was constrained by recent paleomagnetic reconstructions (at 900 Ma by Fu et al. (2015) and at 1.8–1.4 Ga by Xu et al. (2017)).

Other reconstructions linking these blocks (North China and SF-Congo) have been proposed (e.g., Chaves et al., 2018), but they also need to be confronted with new paleomagnetic data and further studies in order to check if, in fact, these blocks were connected in the past and precisely constrain their positions.

If the correct position of these blocks remains controversial, at least, we have evidences that this rift-related magmatism was widely distributed across several blocks and points to a voluminous mafic magmatism occurred during the Tonian, which may be related to break-up attempts of a larger continental piece or a supercontinent of which these blocks were part in the Proterozoic.

6. Conclusions

Based on the results of this study, the following conclusions can be made:

(1) The mafic bodies in the Central Espinhaço are metagabbros, slightly metamorphosed into the greenschist facies, but that still preserve igneous features.
(2) Major and trace element geochemical data indicate that these mafic rocks have a tholeiitic affinity which is typical of continental intraplate mafic magmatism. Additionally, they reveal the evidence of an evolution characterized by fractional crystallization with probable associated crustal assimilation.
(3) Lu–Hf isotopic compositions suggest that during ascent/emplacement, the magma incorporated some continental component.
(4) LA-ICP-MS zircon U–Pb dating indicates that the crystallization ages of these mafic bodies are 895± 3.4 Ma and 896 ± 2.4 Ma.
(5) These mafic rocks were likely emplaced in an extensional regime that occurred during the Tonian, affecting the present east/southeast border of the SFC and the Araçuaí belt. They are correlated to others Tonian-age mafic rocks in the southern SF block (Pedro Lessa and Formiga swarm), indicating that their emplacement may be linked to the same tectonic event. Additionally, on a regional scale, these rocks can be related to the initial rifting that paved the way to the deposition of the Macaúbas basin in the Neoproterozoic.
(6) The mafic Tonian-age bodies in the eastern São Francisco block are similar to those reported in the Congo and North China cratons, therefore, they can indicate records of an extensive mafic magmatism occurred during the Tonian, associated to break-up attempts of a large continental mass or a supercontinent of which these blocks were part in the Neoproterozoic (Rodinia or African Central Block).

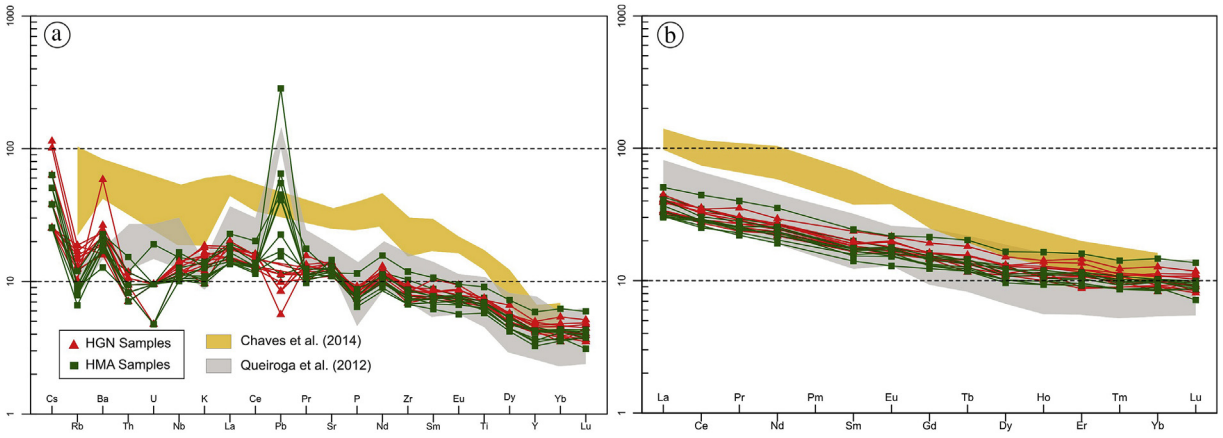

Fig. 17. Comparison between the mafic bodies from Central Espinhaço (samples HGN and HMA) with the metagabbros of the Pedro Lessa Suite (after Queiroga et al., 2012; Chaves et al., 2014) and Formiga Swarm (after Chaves et al., 2014). (a) Primitive mantle-normalized trace element patterns (after Sun and Mcdonough, 1989); (b) chondrite-normalized REE patterns (after Boynton, 1984).

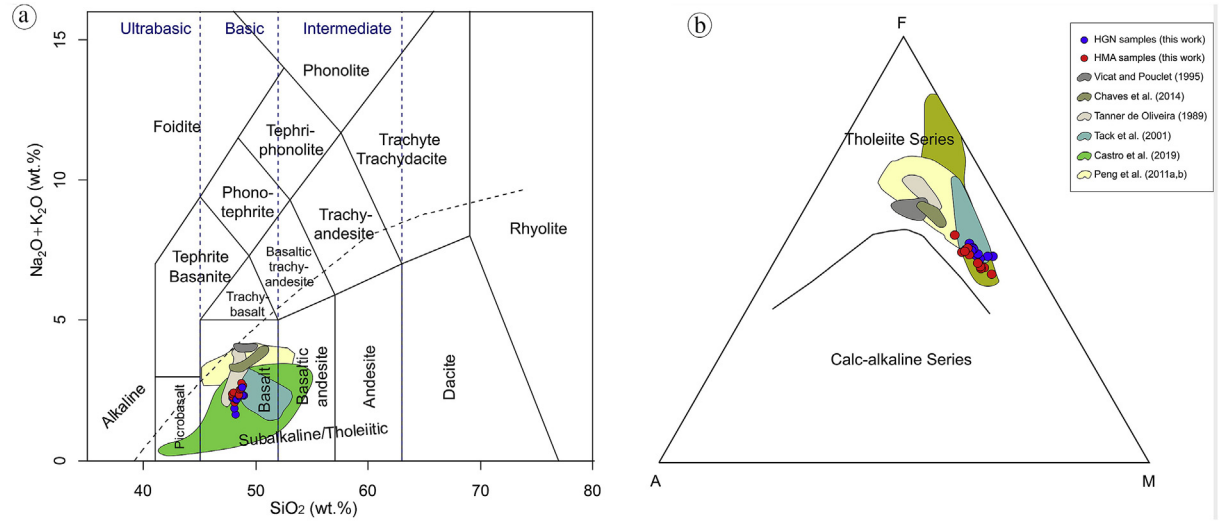

Fig. 18. Geochemical diagrams. (a) TAS diagram from Le Bas et al. (1986); (b) AFM ternary diagram after Irvine and Baragar (1971). Modified from Chaves et al. (2018).

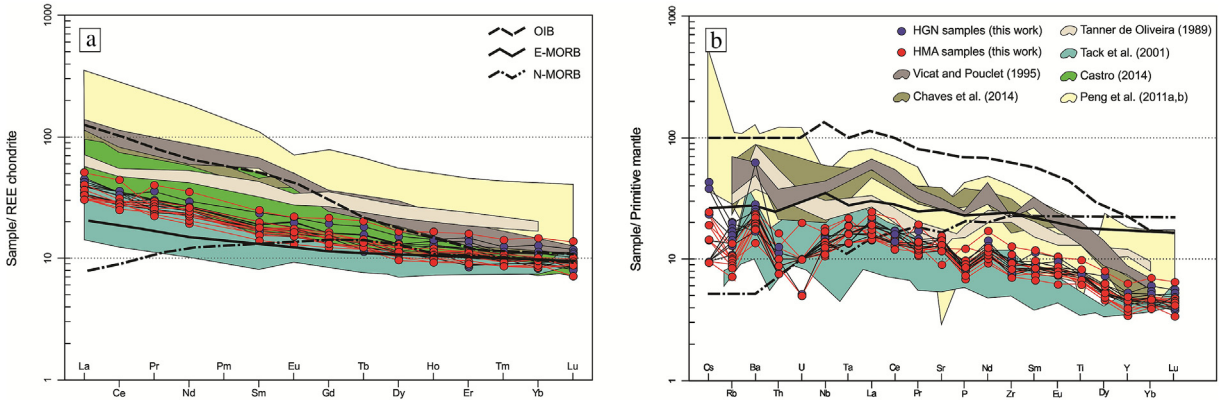

Fig. 19. (a) Chondrite-normalized REE patterns (after Boynton, 1984); (b) primitive mantle-normalized trace element patterns (after Sun and Mcdonough, 1989). Modified from Chaves et al. (2018).

Declaration of competing interest

The authors declare that they have no known competing financial interests or personal relationships that could have appeared to influence the work reported in this paper.

Acknowledgments

The authors acknowledge CAPES, FAPEMIG (APQ-00125-12) and Petrobras (Geotectonic Studies Network) for financial support, the Universidade Federal de Ouro Preto and CDTN (Centro de Desenvolvimento da Tecnologia Nuclear) for institutional support, the Microanalysis Laboratory of the Universidade Federal de Ouro Preto, a member of the Microscopy and Microanalysis Network of Minas Gerais State/Brazil/FAPEMIG for assistance with chemical analyses, and also the Radiogenic Isotope Laboratory DEGEO/UFOP.

Appendix A. Supplementary data

Supplementary data to this article can be found online at https://doi.org/10.1016/j.gsf.2020.02.007.

References

Albert, C., Farina, F., Lana, C., Stevens, G., Storey, C., Gerdes, A., Dopico, C.M., 2016. Archean crustal evolution in the Southern São Francisco craton, Brazil: Constraints from U-Pb, Lu-Hf and O isotope analyses. Lithos 266–267, 64–86.

Alkmim, F.F., Brito Neves, B.B., Alves, J.A.C., 1993. Arcabouço tectônico do Cráton do São Francisco – uma revisão. In: Dominguez, J.M., Misi, A. (Eds.), O Cráton do São Francisco. Reunião preparatória do II Simpósio sobre o Cráton do São Francisco. Salvador, SBG, pp. 45–62 (in Portuguese).

Alkmim, F.F., Kuchenbecker, M., Reis, H.L.S., Pedrosa-Soares, A.C., 2017. The Araçuaí Belt. Springer International Publishing Switzerland. https://doi.org/10.1007/978-3-319-01715-0_14.

Alkmim, F.F., Martins-Neto, M.A., 2012. Proterozoic first-order sedimentary sequences of the São Francisco craton, eastern Brazil. Mar. Petrol. Geol. 33, 127–139.

Almeida, F.F.M., 1977. O cráton do São Francisco. Rev. Bras. Geociencias 7, 349–364 (in Portuguese).

Babinski, M., Pedreira, A.J., Brito Neves, B.B., Van Schmus, W.R., 1999. Contribuição à geocronologia da Chapada Diamantina. In: VII Simpósio Nacional de Estudos Tectônicos, Lençóis, pp. 118–120 (in Portuguese).

Babinski, M., Trindade, R., Pedrosa-Soares, A.C., Martins, M.S., Noce, C.M., Liu, D., 2012. Neoproterozoic glacial deposits from the Araçuaí orogen, Brazil: age, provenance and correlations with the São Francisco craton and West Congo belt. Gondwana Res. 21, 451–465.

Bahlburg, H., Vervoort, J.D., DuFrane, S.A., Carlotto, V., Reimann, C., Cárdenas, J., 2011. The U–Pb and Hf isotope evidence of detrital zircons of the Ordovician Ollantaytambo Formation, southern Peru, and the Ordovician provenance and paleogeography of southern Peru and northern Bolivia. J. S. Am. Earth Sci. 32, 196–209.

Bersan, S.M., 2015. Análise estrutural do embasamento e da cobertura no extremo norte do cinturão de cavalgamentos da Serra do Espinhaço. M.Sc., thesis. Universidade Federal de Ouro Preto, p. 107 (in Portuguese).

Beswick, A.E., Soucie, G., 1978. A correction procedure for metassomatism in Archean greenstone belt. Precambriam Research 6, 235–248.

Bleeker, W., Ernst, R.E., 2006. Short-lived mantle generated magmatic events and their dyke swarms: the key unlocking Earth's paleogeographic record back to 2.6 Ga. In: Hanski, E., Mertanen, S., Rämö, T., Vuollo, J. (Eds.), Dyke Swams - Time Markers of Crustal Evolution. Taylor and Francis/Balkema, London, pp. 3–26.

Bouvier, A., Verboort, J.D., Patchett, P.J., 2008. The Lu-Hf and Sm-Nd isotopic composition of CHUR: constrains from unequilibrated chondrites and implications for the bulk composition of terrestrial planets. Earth Planet Sci. Lett. 273, 48–57.

Boynton, W.V., 1984. Cosmochemistry of rare earth elements: meteorite studies. In: Henderson, P. (Ed.), Rare Earth Element Geochemistry. Elsevier, Amsterdan., pp. 63–114

Carneiro, M.A., Oliveira, A.H., 2005. Tectonic evolution of southern São Francisco Craton: three tectonothermal events based on $^{40}Ar/^{39}Ar$ isotopic data. In: Pinto, M.S. (Ed.), III Simpósio Do Craton São Francisco. Sociedade Brasileira de Geologia, Salvador, pp. 200–203.

Carneiro, C.D., de Almeida, F.F.M., Hasui, Y., Zalán, P.V., Teixeira, J.B.G., 2012. Estágios evolutivos do Brasil no Fanerozóico. In: Hasui, Y., Carneiro, C.D.R., Almeida, F.F.M., Bartorelli, A. (Eds.), Geologia Do Brasil. Beca, São Paulo, pp. 131–137 (in Portuguese).

Castro, M.P., Queiroga, G., Martins, M., Alkmim, F., Pedrosa-Soares, A., Dussin, I., Souza, M.E., 2019. An Early Tonian rifting event affecting the São Francisco-Congo paleocontinent recorded by the lower Macaúbas group, Araçuaí orogen, SE Brazil. Precambrian Res. 331, 105351. https://doi.org/10.1016/j.precamres.2019.10535.

Cederberg, J., Söderlund, U., Oliveira, E.P., Ernst, R.E., Pisarevsky, S.A., 2016. U-Pb baddeleyite dating of the Proterozoic Pará de Minas dyke swarm in the São Francisco craton (Brazil) implications for tectonic correlation with the Siberian, Congo and North China cratons. Geologiska Föreningen 1–17, 00.

Chaves, A.O., Neves, J.M.C., 2005. Radiometric ages, aeromagnetic expression, and general geology of mafic dykes from southeastern Brazil and implications for African-South American correlations. J. S. Am. Earth Sci. 19, 387–397.

Chaves, A.O., Menezes, C.B., de Paula, S.C., 2014. Litoquímica dos diques máficos de Formiga/Pedro Lessa (Brasil) e Kinga-Comba/Sembé-Ouesso (África): marcadores da tafrogênese toniana no craton São Francisco-Congo. Braz. J. Genet. 44, 5–11 (in Portuguese).

Chaves, A.O., Ernst, R.E., Söderlundd, U., Wang, X., Naeraad, T., 2018. The 920–900 Ma Bahia-Gangila LIP of the São Francisco and Congo cratons and link with Dashigou-Chulan LIP of North China craton: new insights from U-Pb geochronology and geochemistry. Precambrian Res. https://doi.org/10.1016/j.precamres.2018.08.023.

Chemale, F., Dussin, I.A., Alkmim, F.F., Martins, M.S., Queiroga, G., Armstrong, R., Santos, M.N., 2012. Unravelling a Proterozoic basin history through detrital zircon geochronology: the case of the Espinhaço Supergroup, Minas Gerais, Brazil. Gondwana Res. 22, 200–206.

Chula, A.M.D., 1996. Caracterização geológica e geoquímica dos metamagmatitos e metassedimentos da região de Planalto de Minas, Município de Diamantina, MG. Ph.D. thesis. Universidade Federal de Minas Gerais, p. 157 (in Portuguese).

Corfu, F., Hanchar, J.M., Hoskin, P.W.O., Kinny, P., 2003. Atlas of zircon textures. In: Hanchar, J.M., Hoskin, P.W.O. (Eds.), Zircon. The Geological Society of America (GSA), Washington, pp. 468–500.

Correa-Gomes, L.C., Oliveira, E.P., 2000. Radiating 1.0 Ga mafic dyke swarms of eastern Brazil and western Africa: evidence of post-assembly extension in the Rodinia supercontinent? Gondwana Res. 3, 325–332.

Costa, A.F.O., 2013. Estratigrafia e tectônica da borda oeste do Espinhaço Central no extremo norte da faixa Araçuaí, Minas Gerais. M.Sc. thesis. Universidade Federal de Ouro Preto, 172pp (in Portuguese).

Costa, A.F.O., 2017. Evolução tectono-estratigráfica da porção norte do Espinhaço Central, Norte de Minas Gerais. Ph.D. thesis. Universidade Federal de Ouro Preto, 220pp (in Portuguese).

Costa, A.F.O., Danderfer, A., 2017. Tectonics and sedimentation of the central sector of the Santo Onofre rift, north Minas Gerais, Brazil. Braz. J. Genet. 47, 491–519.

D'Agrella Filho, M.S., Feybesse, J.L., Prian, J.P., Dupuis, D., N'Dong, G.E., 1996. Paleogmagnetism of precambrian rocks of Gabon, Congo craton, Africa. J. Afr. Earth Sci. 22, 65–80.

D'Agrela-Filho, M.S., Cordani, U.G., 2017. The Paleomagnetic Record of the São Francisco-Congo Craton. São Francisco Craton, Eastern Brazil, pp. 305–320.

Danderfer, A., Dardenne, M.A., 2002. Tectonoestratigrafia da bacia Espinhaço na porção centro-norte do cráton do São Francisco: registro de uma evolução poli-histórica descontínua. Rev. Bras. Geociencias 32, 449–460 (in Portuguese).

Danderfer, A., Lana, C.C., Nalini Júnior, H.A., Costa, A.F.O., 2015. Constraints on the Statherian evolution of the intraplate rifting in a Paleo-Mesoproterozoic paleocontinent: new stratigraphic and geochronology record from the eastern São Francisco craton. Gondwana Res. 28, 668–688.

Danderfer, A., Waele, B.D., Pedreira, A.J., Nalini, H.A., 2009. New geochronological constraints on the geological evolution of Espinhaço basin within the São Francisco Craton – Brazil. Precambrian Res. 170, 116–128.

Deer, W.A., Howie, R.A., Zussman, J., 1992. An Introduction to the Rock-Forming Minerals. Longman, London, 696 pp.

Ernst, R.E., Bleeker, W., Söderlund, U., Kerr, A.C., 2013. Large Igneous Provinces and supercontinents: toward completing the plate tectonic revolution. Lithos 174, 1–14.

Evans, D., Trindade, R., Catelani, E., D'Agrella-Filho, M.S., Heaman, L.M., Oliveira, E.P., Söderlund, U., Ernst, R.E., Smirnov, A.V., Salminen, J.M., 2016. Return to Rodinia? Moderate to high paleolatitude of the Sao Francisco/Congo craton at 920 Ma. In: Li, Z.X., Evans, D.A.D., Murphy, J.B. (Eds.), Supercontinent Cycles through Earth History, vol 424. Geological Society of London, London, Special Publication, pp. 167–190.

Feybesse, J.L., Johan, V., Triboulet, C., Guerrot, C., Mayaga-Mikolo, F., Bouchot, V., Eko N' Dong, J., 1998. The West Central African belt: a model of 2.5-2.0 Ga accretion and two-phase orogenic evolution. Precambrian Res. 87, 161–216.

Fu, X.M., Zhang, S.H., Li, H.Y., Ding, J.K., Li, H.K., Yang, T.S., Wu, H.C., Yuan, H.F., Lv, J., 2015. New paleomagnetic results from the Huaibei Group and Neoproterozoic mafic sills in the North China Craton and their paleogeographic implications. Precambrian Res. 269, 90–106.

Fuck, R.A., Brito Neves, B.B., Schobbenhaus, C., 2008. Rodinia descendants in south America. Precambrian Res. 160, 108–126.

Girardi, V.A.V., Teixeira, W., Mazzucchelli, M., Oliveira, E.P., Correa da Costa, P.C., 2017. Mafic dykes: Petrogenesis and tectonic inferences. In: Heilbron, M., Cordani, U.G., Alkmim, F.F. (Eds.), São Francisco Craton, Eastern Brazil. Springer International Publishing, Switzerlan, pp. 145–171.

Gradim, R.J., Alkmim, F.F., Pedrosa-Soares, A.C., Babinski, M., Noce, C.M., 2005. Xistos verdes do alto Araçuaí, Minas Gerais: vulcanismo básico do rifte Neoproterozóico Macaúbas. Braz. J. Genet. 5, 59–69 (in Portuguese).

Guadagnin, F., Chemale Jr., F., Magalhães, A.J., Santana, A., Dussin, I., Takehara, L., 2015. Age constraints on crystal-tuff from the Espinhaço Supergroup - insight into the Paleoproterozoic to Mesoproterozoic intracratonic basin cycles of the São Francisco Craton. Gondwana Res. 27, 363–376.

Irvine, T.N., Baragar, W.R.A., 1971. A guide to the chemical classification of the common volcanic rocks. Can. J. Earth Sci. 8, 523–548.

Jackson, S.E., Pearson, N.J., Griffin, W.l., Belosova, E.A., 2004. The application of laser ablation-inductively coupled plasma-mass spectrometry to in sito U-Pb zircon geochronology. Chem. Geol. 211, 47–69.

Janoušek, V., Farrow, C.M., Erban, V., 2006. Interpretation of whole-rock geochemical data in igneous geochemistry: introducing Geochemical Data Toolkit (GCDkit). J. Petrol. 47 (6), 1255–1259.
Jensen, L.S., 1976. A new cation plot for classifying subalkalic vocanic rocks. Miscellaneous Paper, Ontário: Div. of mines, 66, 22 pp.
Knauer, L.G., Silva, L.L., Souza, F.B.B., Silva, L.R., Carmo, R.C., 2007. Texto explicativo e mapas Folha Monte Azul. Programa Levantamentos Geológicos Básicos (UFMG/CPRM) Folha SD.23-Z-D-II, 1: 100,000 (in Portuguese).
Kuchenbecker, M., Pedrosa-Soares, A.C., Babinski, M., Fanning, M., 2015. Detrital zircon age patterns and provenance assessment for pre-glacial to post-glacial successions of the Neoproterozoic Macaúbas Group, Araçuaí orogen, Brazil. Precambrian Res. 266, 12–26.
Lana, C., Farina, F., Gerdes, A., Alkmim, A., Gonçalves, G.O., Jardim, A.C., 2017. Characterization of zircon reference materials via high precision U–Pb LA-MC-ICP-MS. J. Anal. Atomic Spectrom. 32, 2011–2023.
Leake, B.E., Wooley, A.R., Arps, C.E.S., Birch, W.D., Gilbert, M.C., Grice, J.D., Hawthorne, F.C., Kato, A., Kisch, H., Krivovichev, V.G., Linthout, K., Laird, J., Mandarino, J.A., Maresch, W.V., Nickel, E.H., Rock, N.M.S., Schumacher, W.V., Smith, D.C., Stephenson, N.C.N., Ungarett, L., Whittaker, E.J.W., Youzhi, G., 1997. Nomenclature of amphiboles: report of the subcommitte of amphiboles of the international mineralogical association, comission on new minerals and mineral names. Am. Mineral. 82, 1019–1037.
Le Bas, N.J., Le Maitre, R.W., Streckeisen, A., Zanettin, B., 1986. A chemical classification of volcanic rocks based on the total alkali-silica diagram. J. Petrol. 27, 459–469.
Li, Z.X., Bogdanova, S.V., Collins, A.S., Davidson, A., De Waele, B., Ernst, R.E., Fitzsimons, I.C.W., Fuck, R.A., Gladkochub, D.P., Jacobs, J., Karlstrom, K.E., Lu, S., Natapov, L.M., Pease, V., Pisarevsky, S.A., Thrane, K., Vernikovsky, V., 2008. Assembly, configuration, and break-up history of Rodinia: a synthesis. Precambrian Res. 160, 179–210.
Li, Z.X., Evans, D.A.D., 2011. Late Neoproterozoic 40° intraplate rotation within Australia allows for a tighter-fitting and longer-lasting Rodinia. Geology 39, 39–42.
Li, Z.X., Zhang, L., Powell, C.M., 1995. South China in Rodinia: part of the missing link between Australia–east Antarctica and laurentia. Geology 23, 407–410.
Ludwig, K.R., 2003. User's Manual for Isoplot/Ex, Version 3.0 – A Geochronological Toolkit for Microsoft Excel, vol 4. Berkerley Geochronology Center, Special Publication, 73 pp.
Machado, N., Schrank, A., Abreu, F.R., Knauer, L.G., Almeida-Abreu, P.A., 1989. Resultados preliminares da geocronologia U-Pb na Serra do Espinhaço Meridional. In: Simp. Bras. de Geol. Belo Horizonte, pp. 171–174 (in Portuguese).
Moreira, H., Lana, C., Nalini Jr., H.A., 2016. The detrital zircon record of an Archaean convergent basin in the Southern São Francisco Craton, Brazil. Precambrian Res. 275, 84–99.
Morimoto, N., 1988. Nomenclature of pyroxenes. Mineral. Mag. 52, 35–550.
Pearce, T.H., Cann, J.R., 1973. Tectonic setting of basic volcanic rocks determined using trace element analysis. Earth Planet Sci. Lett. 19, 290–300.
Pearce, J.A., Norry, M.J., 1979. Petrogenetic implications of Ti, Zr, Y and Nb variations in volcanic rocks. Contrib. Mineral. Petrol. 69, 33–47.
Pedrosa-Soares, A.C., Babinski, M., Noce, C.M., Martins, M., Queiroga, G., Vilela, F., 2011. The Neoproterozoic Macaúbas Group (Araçuaí orogen, SE Brazil) with emphasis on the diamictite formations. In: Arnaud, E., Halverson, G.P., Shields-Zhou, G. (Eds.), The Geological Record of Neoproterozoic Glaciations, vol 36. Memoir of the Geological Society of London, pp. 523–534.
Peng, P., Zhai, M., Li, Q., Wu, F., Hou, Q., Li, Z., Li, T., Zhang, Y., 2011a. Neoproterozoic (900 Ma) Sariwon sills in North Korea: geochronology, geochemistry and implications for the evolution of the south-eastern margin of the North China craton. Gondwana Res. 20, 243–254.
Peng, P., Bleeker, W., Ernst, R.E., Söderlund, U., McNicoll, V., 2011b. U–Pb baddeleyite ages, distribution and geochemistry of 925 Ma mafic dykes and 900 Ma sills in the North China craton: evidence for a Neoproterozoic mantle plume. Lithos 127, 210–221.
Queiroga, G., Dussin, I.A., Martins, M.S., Machado, M.C., Kavashita, K., Chemale Jr., F., 2012. Roteiro de campo – rochas ígneas, 2012. In: Dussin, I.A., Chemale Junior, F. (Eds.), Geologia estrutural e estratigrafia do sistema Espinhaço – Chapada Diamantina e sua aplicação nas bacias Mesocenozoicas de margem passiva brasileira. Projeto Fundep/Petrobras, Belo Horizonte, pp. 184–192 (in Portuguese).
Romano, R., Lana, C., Akmin, F.F., Stevens, G., Armstrong, R., 2013. Stabilization of the southern portion of the São Francisco craton, SE Brazil, through a long-lived period of potassic magmatism. Precambrian Res. 224, 143–159.
Santos, M.M., Lana, C., Sholz, R., Buick, I., Kamo, S.L., Gerdes, A., Condon, D.J., Corfu, F., Tohver, E., Storey, D.S., Basei, M.A.S., Krambrock, K., Fantini, C., 2017. BB zircon – a new Sri Lankan reference material for U-Pb and Hf isotopic laser ablation ICP-MS analysis. Geostand. Geoanal. Res. 41, 335–358.
Schobbenhaus, C., 1996. As tafrogêneses superpostas Espinhaço e Santo Onofre, Estado da Bahia: revisão e novas propostas. Rev. Bras. Geociencias 26, 265–276 (in Portuguese).
Schobbenhaus, C., 1993. O Proterozoico médio do Brasil com ênfase à região Centro-Leste: uma revisão. Ph.D. thesis. Universidade de Freiburg, 166 pp (in Portuguese).
Silva, A.M., Chemale Jr., F., Kuyumjian, R.M., Heaman, L., 1995. Mafic dyke swarms of quadrilátero Ferrífero and southern Espinhaço, Minas Gerais, Brazil. Rev. Bras. Geociencias 25, 124–137.
Silveira, E.M., Söderlund, U., Oliveira, E.P., Ernst, R.E., Menezes, Leal A.B., 2013. First precise U–Pb baddeleyite ages of 1500 Ma mafic dykes from the São Francisco Craton, Brazil, and tectonic implications. Lithos 174, 144–156.
Söderlund, U., Patchett, P.J., Vervoort, J.D., Isachsen, C.E., 2004. The ^{176}Lu decay constant determined by Lu–Hf and U–Pb isotope systematics of Precambrian mafic intrusions. Earth Planet Sci. Lett. 219, 311–324.
Sousa, F.R., Santos, E.L., Jesus, M.T., Medeiros, V.C., 2014. Carta Geológica da Folha Mansidão. Teresina, Serviço Geológico do Brasil, Programa Geologia do Brasil escala 1:1,000,000 (in Portuguese).
Souza, M.E.S., 2016. Caracterização litoestrutural e geocronológica dos metagabros e xistos verdes do Grupo Macaúbas na faixa Terra Branca – Planalto de Minas, Minas Gerais. M.Sc. thesis. Universidade Federal de Ouro Preto, 245 pp (in Portuguese).
Souza, M.E.S., 2019. Evolução geodinâmica dos estágios de rifteamento do Grupo Macaúbas no período Toniano, meridiano 43°30'W, Região Centro Norte de Minas Gerais. Ph.D. thesis. Universidade Federal de Ouro Preto, 204 pp (in Portuguese).
Sun, S.S., Mcdonough, W.F., 1989. Chemical and isotopic systematics of oceanic basalts: implications for mantle composition and process. In: Saunders, A.D., Norry, M.J. (Eds.), Magmatism in the Ocean Basins, vol 42. Geological Society Special Publication, pp. 313–345.
Tack, L., Wingate, M.T.D., Liégeois, J.P., Fernandez-Alonso, M., Deblond, A., 2001. Early Neoproterozoic magmatism (1000–910 Ma) of the Zadinian and Mayumbian groups (Bas-Congo): onset of Rodinia rifting at the western edge of the Congo craton. Precambrian Res. 11, 27–306.
Tanner de Oliveira, M.A.F., 1989. O enxame de diques máficos de Olivença: aspectos geoquímicos e petrogenéticos. Ph.D. thesis. Universidade de São Paulo, 160 pp (in Portuguese).
Teixeira, L.R., 2008. Relatório temático de litogeoquímica. Projeto Barra-Oliveira dos Brejinhos. CPRM-CBPM, Salvador, 29 pp (in Portuguese).
Trompette, R., 1994. Geology of Western Gondwana (2000-500 Ma). Pan-African-Brasiliano aggregation of South America and Africa. Balkema, Rotterdam, 350 pp.
Uhlein, A., 1991. Transição cráton-faixa dobrada: exemplo do Cráton do São Francisco e da Faixa Araçuaí (Ciclo Brasiliano) no estado de Minas Gerais. Aspectos estratigráficos e estruturais. Ph.D. thesis. Universidade de São Paulo, p. 295 (in Portuguese).
Van Achterbergh, E., Ryan, C.G., Jackson, S.E., Griffin, W.L., 2001. Data reduction software for LA-ICP-MS: appendix. In: Sylvester, P.J. (Ed.), Laser Ablation-ICP-Mass Spectrometry in the Earth Sciences: Principles and Applications, Mineralog. Assoc. Canada (MAC) Short Course Series, Ottawa, Ontario, Canada, vol 29, pp. 239–243.
Vicat, J.P., Pouclet, A., 1995. Nature du magmatisme lie a une extension pre-Panafricaine: les dolerites des bassins de Comba et de Sembe-Ouesso (Congo). Bull. Soc. Geol. Fr. 166, 355–364 (in French).
Wang, C., Zhang, J.H., Li, M., Li, R.S., Peng, 2015. Generation of ca. 900–870 Ma bimodal rifting volcanism along the southwestern margin of the Tarim Craton and its implications for the Tarim–North China connection in the early Neoproterozoic. J. Asian Earth Sci. 113, 610–625.
Wiedenbeck, M., Allé, P., Corfu, F., Griffin, W.l., Meier, M., Oberli, F., Von Quadt, A., Roddick, J.C., Spiegel, W., 1995. Three natural zircon standards for U-Th-Pb, Lu-Hf, trace element and REE analyses. Geostand. Geoanal. Res. 19, 1–23.
Wilson, M., 1989. Igneous Petrogenesis. Springer, Dordrecht, 466 pp.
Wood, D.A., 1980. The application of a Th-Hf-Ta diagram to problems of tectonomagmatic classification and to establishing the nature of crustal contamination of basaltic lavas of the British Tertiary volcanic province. Earth Planet Sci. Lett. 50, 11–30.
Xu, H., Yang, Z., Peng, P., Ge, K., Jin, Z., Zhu, R., 2017. Magnetic fabrics and rock magnetism of the Xiong'er volcanic rocks and their implications for tectonic correlation of the North China Craton with other crustal blocks in the Nuna/Columbia supercontinent. Tectonophysics 712–713, 415–425.
Zhu, W., Zheng, D., Shu, L., Ma, D., Wan, J., Zheng, D., Zhang, Z., Zhu, X., 2011. Geochemistry and SHRIMP U–Pb zircon geochronology of the Korla mafic dykes: constrains on the Neoproterozoic continental breakup in the Tarim Block, northwest China. J. Asian Earth Sci. 42, 791–804.